Archives of Computational Methods in Engineering manuscript No.
(will be inserted by the editor)

Computational modeling of tumor-induced angiogenesis

Guillermo Vilanova · Ignasi Colominas · Hector Gomez

Received: date / Accepted: date

Abstract Angiogenesis is the growth of new capillaries from preexisting ones. The ability to trigger angiogenesis is one of the hallmarks of cancer, and is a necessary step for a tumor to become malignant. This paper discusses computational modeling of tumor-induced angiogenesis with particular reference to mathematical modeling, numerical simulation, and comparison with experiments. We describe the basic biological phenomena associated with angiogenesis, and discuss how they can be incorporated into mathematical models. We emphasize the crucial role of numerical methods for model development. In particular, computational methods for tumor angiogenesis need to be geometrically flexible and capable of dealing with higher-order derivatives, which suggests isogeometric analysis as an ideal candidate. Finally, we propose an algorithm based on graph theory as a potential method for quantitative validation of tumor angiogenesis models.

Keywords Angiogenesis · Mathematical modeling · Computational methods

1 Introduction

Cancer is the second cause of death in the world, just behind cardiovascular diseases (see figure 1 left). According to the last estimation from the World Health Organization performed in 2012 [76], approximately 8.2 million people died from cancer, that is, 15% of all deaths worldwide. As highlighted in the right-hand side of figure 1, the global fight against cancer is hindered by the different cancer burden and cancer types among regions. The number of people that die from cancer varies greatly between different income countries. Population aging and lifestyle —including smoking, diet, and physical activity— are among the main reasons of cancer deaths in the high and upper-middle income countries, while insufficient access to treatments and late diagnosis are the causes for high cancer mortality in lower-middle income countries. The high burden of infections and parasitic diseases in low income countries explain their lower cancer mortality. Despite the amount of funding and research in the field, these figures increase year after year, probably boosted by the growth and aging of the population. All these facts highlight the importance of a

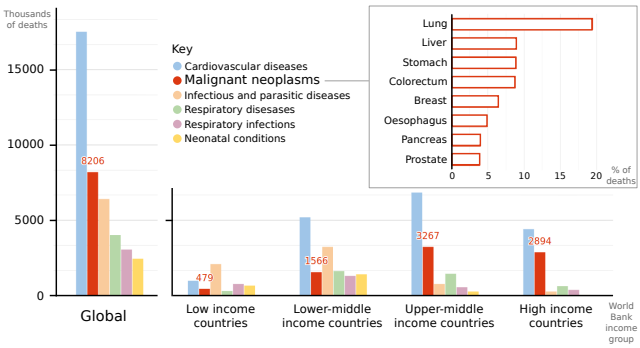

Fig. 1 Leading causes of death by World Bank income group [212]. After heart diseases, cancer is the leading death cause globally and in the upper-middle and high income countries. Inset: Percentage of cancer deaths over global malignant neoplasm deaths by cancer type. Data source: Latest estimates by the World Health Organization [76]

G. Vilanova (✉) · I. Colominas
Departamento de Métodos Matemáticos e de Representación
Grupo de Métodos Numéricos en Ingeniería
Universidade da Coruña
Campus de Elviña, 15071, A Coruña, Spain
E-mail: gvilanovac@udc.es

H. Gomez
School of Mechanical Engineering, Purdue University, 585 Purdue Mall, West Lafayette, IN 47907, USA

community of interdisciplinary researchers coming from all the branches of science and engineering equipped with all kinds of tools to fight cancer.

1.1 How cancer is understood nowadays

At present, we understand cancer as a group of diseases —more than a hundred— that share common characteristics: The uncontrolled proliferation of cells and their ability to invade other tissues and continue there with their abnormal proliferation. Each cancer is different from the others in many aspects and they are usually named after the host tissue in which they develop at first, as in breast cancer, prostate cancer, or lung cancer. Cancer is originated by a single abnormal cell [205] that acquires malignant characteristics through mutations, that is changes in its DNA, . This process, called *carcinogenesis*, is complex and may take years or decades to complete. The consequence of carcinogenesis is usually the creation of solid masses or tumors, formed by cancer cells that multiply rapidly, even ignoring the anti-growth signals sent by the body. Tumors grow and develop going through a set of increasingly-malignant stages. Remarkably, tumors can gain the ability to invade nearby tissues and create secondary tumors in distant organs using the vasculature as a means of transport. It is at this point, when the tumors are more malignant, that cancer is more lethal. However, there is not a single reason why cancer kills, but it depends on the type of cancer. One reason is the loss of function of a vital organ (or organs) due to the uncontrolled and abnormal growth of the tumor (or tumors). For instance, lung cancer may spread until there is not enough healthy tissue to absorb oxygen or colorectal cancer may expand into the lumen of the intestines blocking digestion. Also, the fine tuned regulation of some chemicals in the body may be unbalanced by a tumor located in the organ that produces them. For example, the amount of calcium in blood may be risen by bone cancer causing unconsciousness and eventually death.

In most types of cancer, luckily, from carcinogenesis until cancer becomes a real threat to life, cancer cells have to overcome several natural barriers that prevent tumor growth. Continuous research has deepened the knowledge in such barriers and, nowadays, they are understood as opportunities to develop treatments that delay or halt tumor growth. For example, tumors can not grow beyond a certain size until cancer cells gain the ability to promote angiogenesis, that is, the creation of new blood vessels from the pre-existent ones.

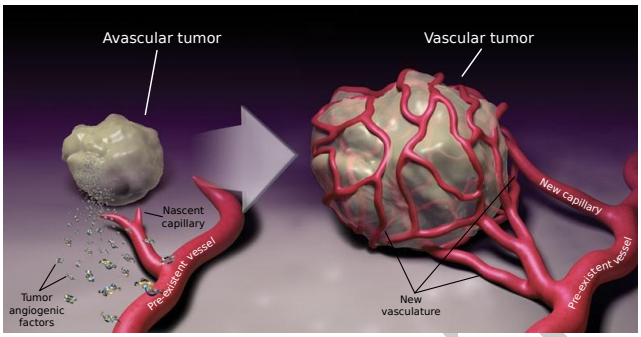

Fig. 2 The angiogenesis switch. Tumors are able promote angiogenesis, the growth of new vessels from pre-existing ones, through signaling. The nutrient from the new capillaries triggers a virtually unbounded tumor growth and the possibility to metastasize using the circulatory system. Adapted from [1]

1.2 The role of angiogenesis in cancer

Certain types of cancer form solid tumors of aberrant, mutated cells. These cells, that proliferate in a high-rate manner, aggregate in solid masses that grow at the expense of the resources of their surroundings. At this stage of tumor growth (called the *avascular stage*), cancer cells depend on diffusion mechanisms to obtain nutrients. However, when the tumor has grown up to a certain size, not larger than 2 mm radius in experiments [80], its global growth stops. This occurs due to the scarceness of nourishment and oxygen that does not even cover the demands for maintaining the basic cell processes in the core of the mass. Tumors may stay dormant in this stage for years and only grow further if cancer cells acquire the ability to induce angiogenesis. In order to promote vessel growth, tumor cells (and even non-cancerous cells from the tumor micro-environment) release chemical signals, called *tumor angiogenic factors* (TAFs), that alter the phenotype of the endothelial cells that line nearby capillaries. As a result, new capillaries grow towards the tumor and provide nourishment to cancer cells. Thus, angiogenesis enables a boost in tumor development, the so-called *angiogenic switch* (see figure 2), moving the tumor to the vascular phase and endowing cancer cells with nutrients and oxygen to grow without limits and with new ways of migration to other tissues or organs of the body.

The realization of the key role of angiogenesis has led to the development of antiangiogenic therapies. Although this will be explained later in the paper, we anticipate here that these therapies have not achieved the expected results yet. Arguably, an emerging paradigm in medicine called *predictive medicine* might change radically cancer investigation and may be the tool to unravel the problems with antiangiogenic therapy.

1.3 Predictive medicine

Cancer is a disease with a high morbidity and mortality rate, thus it is hardly surprising that many people devote their efforts and work to deepen the knowledge we currently have on cancer, comprehending better the mechanisms involved and thereby being able to better diagnose and create new treatments. This research, as well as the clinical practice, is usually developed by groups composed by physicians and biologists. They follow the diagnostic paradigm, which is heavily based on the experience of the physicians and on statistical data of the effect of the treatments on large groups of individuals. In the last decades, however, a new paradigm based on mathematical modeling and computation has been proposed: predictive medicine. Its aim is to predict the emergence, development, and consequences of a disease, as well as to enhance current treatments and propose new ones.

This new approach has been successfully applied to cardiovascular diseases [191] and orthopedics [192], and it has recently been applied to oncology [58, 84, 143, 170, 219]. In particular, the literature shows a boost in the last years in the number of new mathematical models and computational methods for tumor-induced angiogenesis, which we review in the present work.

1.4 Overview of the paper

The remaining sections of this paper are organized as follows: First, section 2 explains the biological background of angiogenesis. Then, in section 3 we detail the state of the art of mathematical modeling of tumor-induced angiogenesis. Section 4 deals with the computational challenges that arise from these models and presents a promising flexible method to overcome some of these problems. Finally, we showcase the method with several results in section 5 and we summarize and give some final thoughts in section 6.

2 Biology background

We open this section giving a background of the process of cancer initiation and growth, the role of the tumor environment and angiogenesis, and the main treatments used nowadays. Then we focus on the biology of angiogenesis, explaining this process both under physiological and tumor-induced conditions. We also analyze the characteristics of tumor vessels and the new different approaches to antiangiogenic treatments.

2.1 Cancer growth and spread

2.1.1 Carcinogenesis

Carcinogenesis, also called *tumorigenesis*, is the process whereby normal cells acquire the capabilities to become cancer cells. These capabilities are usually gained through mutations, but also by non-mutational changes in mechanisms regulating gene expression —those exerting the transcriptional control; for example whether a gene should be transcribed or not or the transcription velocity needed under certain circumstances. However, in the rest of the document, we will refer to both of them just as *mutations* for the sake of clarity. There are many genes known to be involved in carcinogenesis and, surely, many more still unknown.

The first step towards cancer development starts when a cell undergoes a mutation in one of these genes and the machinery which was supposed to eliminate this cell through the apoptotic program fails in its function. This occurs because the mentioned machinery is not perfect. Notwithstanding, this fact does not mean all cells that evade this natural barrier to defective cells lead to cancer formation. Most of the cells that elude the machinery either have minor changes in chromosomes —mutations in genes that do not jeopardize cell integrity— or the alterations are so severe that the cell is not viable and it is doomed to die. However, in the rare cases a mutation results in a viable cell with altered functions or characteristics it may mean a step towards evolution or a step towards a disease like cancer.

The order of magnitude of the number of mutations that an individual may suffer through his/her life is 10^{10} [5]. The probability that one of these mutations affects the machinery that controls cell cycle is so high that, if only one mutation was required to develop cancer, we would be non-viable organisms. However, carcinogenesis is a multi-step process that usually takes a long time —years or decades— to be fully completed because normal cells only acquire a malignant phenotype through the accumulation of several mutations [126]. For example, an individual who has been exposed to exogenous risk factors may develop clinically detectable cancer 20 years after. In fact, many cancers never develop, because carcinogenesis starts late in the life of an individual, who may die earlier due to other reasons. It is remarkable that as life expectancy has increased in the last centuries, cancer incidence has grown, demonstrating that aging is a cancer risk factor.

For these reasons, Hanahan and Weinberg in the superb series of papers [90, 91] highlighted that one of the main enabling characteristics to develop cancer is genome instability and mutation of cells. They also

added to these characteristics the ability of tumors to promote inflammation and the aid from the recruited cells of the tumor micro-environment. The aim of these papers was to collect all the capabilities that cells must acquire through mutations to become malignant. They called them *The Hallmarks of Cancer* and are the following: Sustaining proliferative signaling, evading growth suppressors, resisting cell death, enabling replicative immortality, inducing angiogenesis, activating invasion and metastasis, reprogramming of energy metabolism, and evading immune destruction. They are usually acquired at different times and some of them define the stage at which the tumor is.

2.1.2 The stages of tumor growth

As a result of carcinogenesis, there is a viable mutated cell, often called the *renegade cell* [205], which has acquired partially or totally one or more hallmarks. The cell and its daughters proliferate generating clonal expansions that inherit the hallmarks. The same process may be repeated triggered by carcinogenic agents leading to increased malignant subgroups of cells, each of them with different gathered traits. Thus, a heterogeneous mass of aberrant cells originates a tumor.

Tumor growth may be understood as a multistage process. For many tumors, the first of these stages is avascular growth. At this stage, the tumor relies on diffusion mechanisms to get nutrients and to remove the waste products of the cell activity through nearby blood and lymphatic vessels. However, as the tumor grows, diffusion mechanisms become insufficient to maintain the high proliferation rate of tumor cells. At this point, the tumor usually resembles a spheroid where those cells located far from the vessels, that is, towards the center of the spheroid, enter non-proliferative hypoxic states or die from anoxia, starvation, or metabolic poisoning. As a consequence, solid avascular tumors present a characteristic cell-layered configuration, as shown in figure 3. The outermost cells form a thin layer (2 to 3 cells wide), called the *proliferative rim*, where tumor cells have access to nutrient delivered by pre-existent, extratumoral capillaries. This layer envelops the so-called *hypoxic zone*, where the amount of nourishment is above a deadly threshold, but it is not enough for cell proliferation. Those cells in the hypoxic zone enter a quiescent state, only altered when the levels of nutrients vary. Finally, if the tumor is big enough, there is no means for the cells at its core to obtain nutrients. These cells necrose[1] and form a *necrotic core*. Contrary to apoptosis, necrosis generates toxic wastes and, because there is no means to remove the wastes, the toxicity promotes malignancy or necrosis in the surrounding cells. Hence, diffusion-limited growth imposes a threshold in the maximum diameter of an avascular tumor (usually between 1 and 2 mm), for which the cell subdivision rate at the proliferative rim is balanced with cell death rate at the necrotic core [80]. The tumor may be years or decades immersed in the avascular stage [81] without causing any harm to the host tissue.

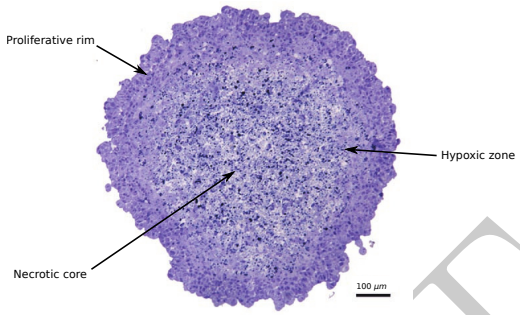

Fig. 3 Section of an avascular tumor. A non-invasive avascular tumor reaches a stable configuration with three main distinguished regions: The proliferative rim, the hypoxic zone, and the necrotic core. Adapted from [221]

Eventually, a tumor cell may find a way to access nutrients and to eliminate wastes. One of these ways (first hypothesized by Folkman in 1971 [80]) is to create its own blood supply through angiogenesis. The genomic instability of tumor cells may lead to daughter cells that have gained the ability to control the balance of angiogenic factors (one of the above-mentioned hallmarks), for example under hypoxic conditions. As a consequence, the tumor may overcome the size-limited avascular growth and enter the so-called vascular stage. This step, the angiogenesis switch [29, 81], is often related to a malignant state of the tumor, as cell proliferation is no longer limited and cells may enter the bloodstream and migrate to any part of the body, attaining the tumor invasive-metastatic stage. Due to this key role played by angiogenesis in tumor growth, we anticipate here that controlling angiogenesis is the aim of some cancer treatments: the antiangiogenic therapies. Another way through which tumors get access to nutrients is by co-opting pre-existing vessels; that is, cancer cells migrate towards vessels and proliferate around them. Usually, the high pressure that cancer cells exert produces the collapse of the vessel, returning thus the tumor to an avascular stage.

Invasion and metastasis is usually the last step of tumor growth and, typically, the cause of death. To achieve this stage cells undergo the so-called *invasion-metastasis cascade* [77, 190]. This step is also the most complex one,

[1] Necrosis is the premature death of cells caused by external factors. In contrast to apoptosis, which is a naturally occurring cause of cellular death, necrosis is almost always detrimental.

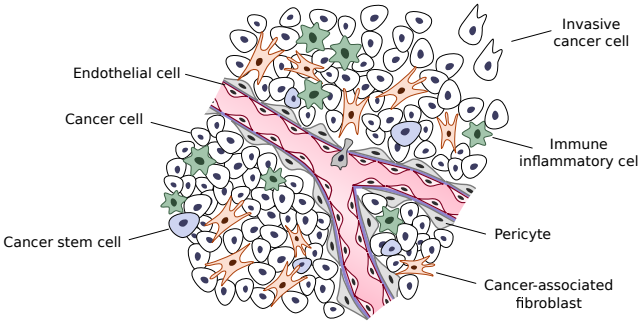

Fig. 4 Tumor stroma. Cancer cells recruit other cells from their micro-environment to form the tumor stroma. This stroma includes cancer cells, cells associated to newly formed vessels, activated fibroblasts, and inflammatory infiltrates

as cancer cells must survive in alien micro-environments from where they were originated and for long times in many cases.

2.1.3 Tumor stroma

One of the changes in the way cancer is understood nowadays is to consider tumors composed, not just by the cancer cells, but also by their micro-environments. If a tumor spreads beyond the avascular phase it is due to the recruitment of the neighboring cells which are present in the extracellular matrix (ECM). These cells are not malignant *per se*, but tumors use them for their own purposes, commonly attracting and controlling them through signaling. Generally, the tumor-recruited cells are referred to as *tumor stroma*, because they are part of the supporting normal tissues. The tumor stroma is composed at least by the following elements: cancer cells, cells associated to the newly formed blood and lymphatic vessels, activated fibroblasts or cancer-associated fibroblasts, and inflammatory infiltrates (figure 4).

The realization of the key role played by the tumor stroma in cancer development has implied a significant step in understanding this disease. What is more, the core of some new cancer therapies derived from the regulation of the cancer stroma. For example, as explained below, antiangiogenic therapy aims to control the development of vessels that form part of the malignant stroma. Also, some treatment failures may be attributed to the reductionist view of targeting only cancer cells or only a sub-type of them.

2.1.4 The main treatments

Some of the main treatments for cancer are surgery, radiation therapy, chemotherapy, immunotherapy, targeted therapies, hormonal therapies and antiangiogenic therapies. Usually these treatments are not used exclusively, but combined. Further information about cancer treatments can be found in [41, 75, 102, 114].

The antiangiogenic treatment is the most relevant for this paper. Although antiangiogenic therapies are frequently used in some types of cancer, e.g., hepatocellular carcinoma, they have not met physicians' expectations, specially when used as a monotherapy. There are several computational efforts directed at unveiling the reasons for their relatively modest success [154, 184, 213].

2.2 Blood vessel growth. Angiogenesis

2.2.1 The circulatory system

The circulatory system serves as a means of oxygen and nutrient delivery, waste products' disposal from the cell cycle, long distance signaling transport, such as hormones, and immune surveillance. In addition, it plays a central role in organogenesis. The circulatory system is often seen as composed by the cardiovascular system and the lymphatic system. The major components of the former are the blood, a fluid chiefly consisting of platelets, blood cells, and plasma; the heart, a muscle responsible for pumping blood; and the blood vessels, the ducts that span the body and through which blood flows. The lymphatic system is also formed by a fluid, the lymph, and by vessels, the lymphatic vessels. Its role is more related to the immune system.

All cells in our body, apart from rare exceptions such as corneal cells, rely on the circulatory system for survival. Thus, it is necessary for the system to span the whole body. The vessels of the circulatory system are formed by different layers, whose number and purpose varies with the caliber and function of the vessel. The innermost layer, the endothelium, is formed by the main component of the vascular (and lymphatic) system: endothelial cells. These cells line blood vessels forming a tube, the lumen, and are usually at a quiescent state. Blood vessels are enveloped by pericytes whose main function is to stabilize endothelial cells, but also collaborate in other activities such as regulating the permeability in certain organs (e.g., blood-brain barrier). Pericytes and endothelial cells share a common basement membrane and the three of them (and occasionally smooth muscle cells) are the main components of capillaries. Greater vessels are formed by increasing number of layers that provide them with support to accommodate the dynamic loads of the flowing blood.

2.2.2 Mechanisms of vessel growth

The functions carried out by the circulatory system are essential to sustain life, therefore the generation and maintenance of such an intricate and complex system is vital. It is during embryogenesis when the blood and the blood vessel network develop. First, through a process known as vasculogenesis, endothelial cell precursors migrate from the bone marrow towards the corresponding emplacement and differentiate into endothelial or blood cells, forming a plexus. Afterwards, the vascular bed is extended and remodeled via several mechanisms such as angiogenesis [44] and intussusception or splitting angiogenesis [115]. Then, in adult life, physiological vasculogenesis, angiogenesis, or intussusception appear at very specific, tightly regulated events and only for a short time span, usually days or weeks. Examples of such events are the female reproductive cycle or tissue repair, as in the wound healing process. Due to the importance of the vascular system, it is not surprising that defective maintenance of blood vessels or deregulation of its growth are associated with a number of diseases. When there is an inadequate vessel maintenance or a downregulated growth, the absence of blood vessels may affect the tissue repairing program, as in ischemic chronic wounds in diseases such as stroke, obesity-associated disorders, or myocardial infarction. On the other hand, an abnormal remodeling or upregulated growth, may promote inflammatory diseases, age-related macular degeneration, or cancer, just to name a few. For a longer list of diseases related to blood vessel maintenance and formation, the reader is referred to [45]. In particular, in cancer, tumors gain access to the vasculature using several mechanisms:

- Using existing blood vessels:
  - **Vessel co-option**: Cancer cells engulf existing blood vessels [117].
  - **Vessel translocation**: Vessels are attracted towards the tumor location [113].
- Creating new blood vessels:
  - **Angiogenesis**: It is the formation of new blood vessels from pre-existing ones.
  - **Postnatal vasculogenesis**: It is the formation of new blood vessels through the migration from bone-marrow and differentiation of endothelial precursor cells.
  - **Intussuception or splitting angiogenesis**: It is the splitting of one vessel into two through the formation of a transluminal pillar and its extension [37, 115].
  - **Mosaic vessel formation**: It is the incorporation of cancer cells among the endothelial cells of the vessel walls.
  - **Vasculogenic mimicry**: It is the transdifferentiation of cancer cells into endothelial cells.

As it might be expected, tumors may exploit several of these mechanisms along their growth, even at the same time. However, among all of them, angiogenesis is assumed to account for a substantial fraction of vessel growth and it will be the objective of study here. It is worth noting that there is not full agreement between these terms and some authors use *angiogenesis* as a general term which includes all these mechanisms of vessel creation and growth. Here, however, we will use it as the specific term defined above.

2.2.3 The process of tumor angiogenesis

Endothelial cell quiescence is maintained by a tightly controlled balance between chemicals that promote angiogenesis (proangiogenic factors) and those that inhibit angiogenesis (antiangiogenic factors). Despite this tight control, tumors are able to trigger angiogenesis. Tumor angiogenesis is a complex phenomenon governed by intertwined molecular mechanisms whose main components are the so-called tumor angiogenic factors (TAFs). The latter are chiefly soluble molecules, released by hypoxic cancer cells and their malignant micro-environment. There are more than twelve known TAFs and many others still under research. In addition, there are complex interplays among them that are still being disentangled.

Angiogenesis, as shown in figure 5, may be described as a multistage process composed of the following steps: activation, initiation of the sprout, growth of the capillary, and finalization of the process [46, 79, 157, 206]. The activation starts when the equilibrium of the pro- and anti-angiogenic factors is disturbed near the endothelial cells that line the blood vessels. The disequilibrium may be caused by the arrival of tumor proangiogenic factor molecules that diffuse from the hypoxic tumor cells and bind to the receptors of endothelial cells. Well-known examples of these factors are vascular endothelial growth factor (VEGF), fibroblast growth factor (FGF), angiopoietin 2 (Ang-2), or chemokines. Cells affected by these tumor angiogenic factors are activated to become the leading cells of the incipient sprout: the tip endothelial cells (TECs). However, there is a mechanism, called *lateral inhibition*, that prevents the formation of several sprouts in the same region [94]: even though several neighboring endothelial cells may sense the disequilibrium of angiogenic factors, only one of them changes its phenotype from quiescent to migratory and becomes a TEC. The remaining cells, instead, change their phenotype to a proliferative one. The latter, referred to as stalk endothelial cells (SECs), will play a role in the elongation of the sprout, as explained below. The key

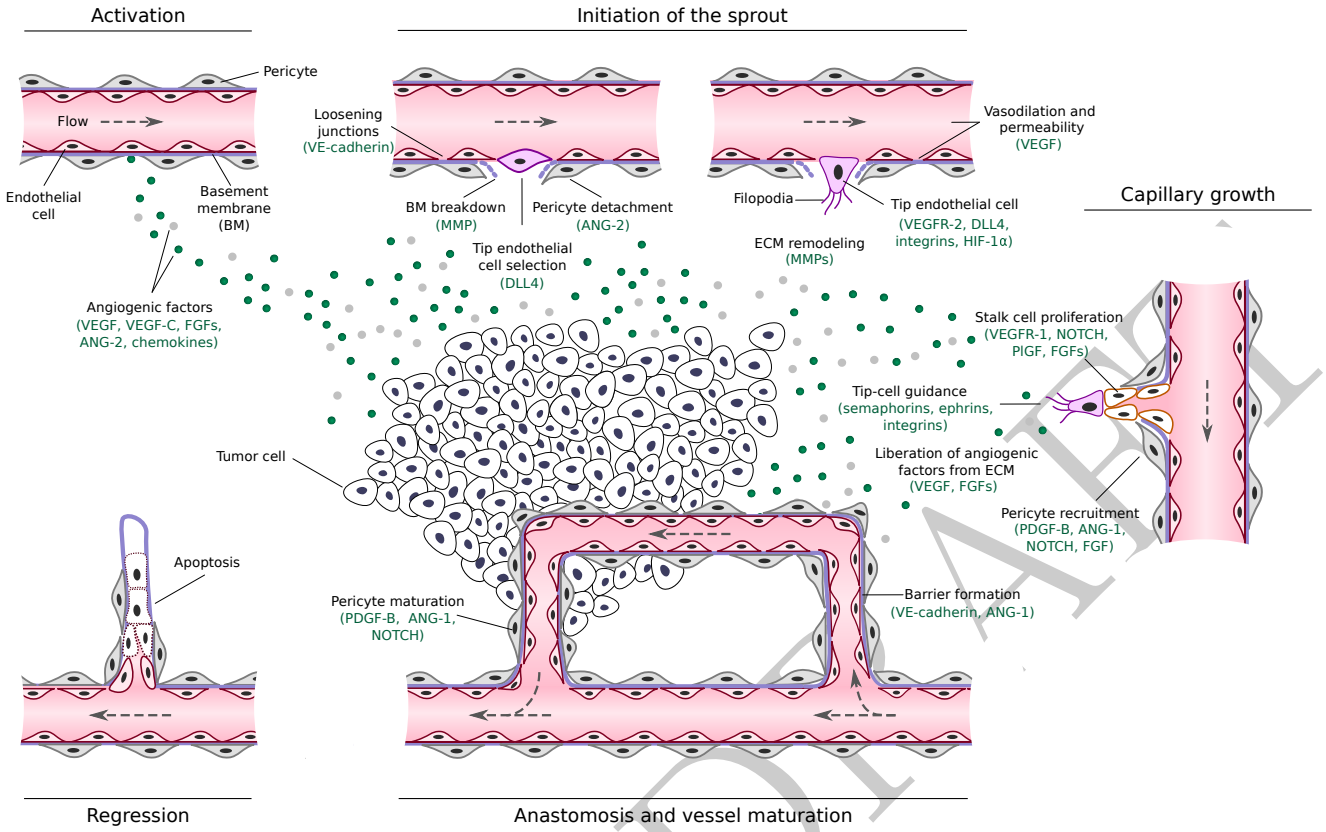

Fig. 5 The angiogenic process. Angiogenesis starts with the activation of tip endothelial cells by tumor angiogenic factors. The incipient sprout, once liberated from the capillary coverage, grows towards the source of tumor angiogenic factors. The capillary elongates by the proliferation of stalk endothelial cells. The growth continues until two capillaries anastomose. The new vessel maturates and blood flows through it irrigating the tissue. Additionally, in the absence of stimuli, non-mature capillaries may also regress

molecular players of lateral inhibition are the Delta-like ligand 4 (Dll-4) and its receptor Notch-1. In brief, TAFs activate the expression of Dll-4 which binds to the membrane Notch-1 receptors of the adjacent cells. Those cells whose Notch-1 receptors get activated become SECs and only one, the first to express Dll-4, becomes a TEC. By the end of the activation phase, endothelial cells have changed their phenotype and are prepared to create a new sprout. They are, however, still confined by the mural cells and the basement membrane.

The initiation of the sprouts starts with the liberation of endothelial cells. First, the pericytes that enwrap the vessels, by means of Ang-2, detach from the region of the incipient sprout. Then, tumor stromal cells release matrix metalloproteinases (MMPs) that produce a proteolytic breakdown of the basement membrane that envelopes the endothelial cells. MMPs also liberate cleaved TAFs from the extracellular matrix. Once the basement membrane is degraded, the endothelial cells loosen their junctions (VE-Cadherin), the nascent vessel dilates, and a provisional ECM is laid out to facilitate migration. TECs develop slender cytoplasmic protrusions, called *filopodia*, rich in receptors that enhance the detection of the stimuli that guide the migration [85]. The adjoining SECs follow the first movements of the TEC out of the capillary.

The growth of the capillary includes the guidance of the TEC and the elongation of the capillary. TECs are guided at least by three different mechanisms, namely, chemotaxis, haptotaxis, and mechanotaxis. The first refers to the movement along a gradient of soluble molecules, in this case, TAFs such as VEGF or FGF. Haptotaxis and mechanotaxis also contribute to establish the growth direction through focal adhesion sites and mechanical forces, respectively. Lately, it has been hypothesized that endothelial cells compete for the TEC position as the capillary grows [107]. Behind the TEC, SECs are continuously dividing stimulated by angiogenic factors, promoting thus the elongation of the capillary. Meanwhile, endothelial cells form a lumen, allowing blood to flow. Furthermore, they attract smooth muscle cells and pericytes, that provide support to the capillary. This last process, called maturation, is usually defective in tumor-induced capillaries.

The growth continues until the lumina of two capillaries fuse forming a loop that allows blood to flow. This phenomenon is called *anastomosis*. When this happens, endothelial cells revert their phenotype to a quiescent one (also called *phalanx* phenotype) and recruit more pericytes that help to maintain this phenotype through signaling. Also, both types of cells create a shared basement membrane and the endothelial cells reestablish their junctions. The growth may also be stopped if the driving stimuli end. In tumor angiogenesis, this point is reached when the hypoxic cancer cells are supplied with enough nutrients and oxygen as to become normoxic. The capillaries promoted by tumors are usually slightly different from those created under normal circumstances. Specifically, they become dependent on TAF presence, thus, when the stimuli are no longer present, the capillaries regress. In addition, the high pressure inside the tumor combined with the weakness of the vessels may make them collapse. Finally, the regrowth of the capillaries is common in tumor development and it is done at a faster speed aided by the scaffold of basal lamina left behind by the regression of the vessels [130].

2.2.4 Characteristics of tumor vessels

As a result of the angiogenesis switch, the once growth-stable avascular tumor has turned into an unstable, vascular, and malignant tumor pervaded with capillaries. However, as shown in figure 6, the new capillaries are defective in several senses [15]. Overexpression of proangiogenic factors and/or underexpression of antiangiogenic factors lead to the formation of a new vasculature that is structurally abnormal. At the anatomical level, the precocious and disorganized capillary sprouting and endothelial cell proliferation, combined with localized events of regression and regrowth, plus the increased vascular shunting and collapse results in a marked loss of the strict hierarchy that characterizes the normal vasculature. At the cellular level, endothelial cells show an irregular and disorganized morphology, that even present long cytoplasmatic projections that transverse the capillary lumen. The association between endothelial cells is weak, leading to loose connections between cells. The perivascular cells that ensheathe normal vessels are loosely attached or even absent in tumor-induced vessels. The vascular membrane is unusually thick in some tumors or very thin or absent on others.

These anatomical and cellular abnormalities have drastic influences at the functional levels of the new vasculature:

– **Heterogeneity in blood flow.** Structural defects promote spatial and temporal heterogeneous blood flow. Furthermore, the flow is often redundant in closed and blind loops.
– **High interstitial pressure.** Defects at the cellular levels confer leakiness to the vasculature. Thus, the intravascular fluids and plasma easily extravasate, increasing the interstitial pressure. In addition, the absence of functional intratumoral lymphatic vessels results in impaired clearance of the fluid. The high interstitial pressure hinders the delivery of systemically administered therapies.
– **Regional hypoxia.** Tumors present local regions of hypoxia due to several factors such as vascular collapse, regression and regrowth events, regional poor perfusion, and high interstitial pressure. As cancer cells are more resistant to hypoxia than normal cells, hypoxia promotes their malignant phenotype, facilitating, for instance, their ability to form metastasis.
– **Acidosis.** It is caused by the byproducts of necrosis that cannot leave the tumor because of the faulty transport functionality of the vasculature. Acidosis compromises the cytotoxic functions of immune cells that infiltrate the tumor, enhancing the malignant phenotype.

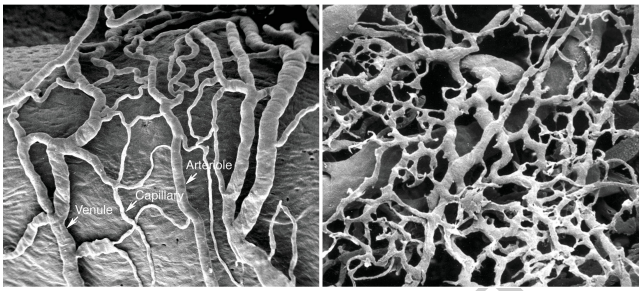

Fig. 6 Physiological versus tumor vessels. Unlike vessels created under physiological conditions (left panel), tumor vessels (right panel) show a clear loss of the vessel hierarchy and structure, a marked aberrant morphology, and disorganized and abundant sprouting. Reproduced from [133]

2.2.5 Antiangiogenic treatments

Since Folkman hypothesized the angiogenic switch, antiangiogenic therapy has been a promising treatment against cancer. In the last decades, different kinds of inhibitors of angiogenesis have been developed, being most of them VEGF blockers or multi-targeted tirosine-kinase receptor inhibitors. Some of them, as bevacizumav or sorafeniv, have been approved for clinical use against specific types of cancer and usually in combination with chemotherapy.

However, despite their success in pre-clinical trials, the translation of most angiogenic inhibitors to clinical practice has not resulted as expected: although in some

cases the disease-free progression has increased, the overall survival did not. There are many hypotheses that try to explain this general failure. Most of these hypotheses are based on the differences between the pre-clinical and the clinical settings, the unknowns in dose amount, or the dose timing. Also, some patients are refractory to the treatment and many others develop resistance to it. For example, Dvorak and colleagues [141] have detected that anti-VEGF therapy is effective only at certain stages of vessel growth, and is refractory otherwise. Recently, Jain and co-workers have hypothesized that the little efficacy of antiangiogenic therapies may be due to an excessive pruning of the vasculature [87, 104, 105]. High doses or treatments over long time spans prune the vasculature too much and promote hypoxia in the tumor, which in turn increases the malignancy of tumor cells and their resistance to radiotherapy and chemotherapy. Thus, excessive pruning leads to more aggressive forms of cancer. They propose that the aim of antiangiongenic therapy should be instead the normalization of the vasculature, such that the adjuvant therapies that are administered systemically are not impaired by a defective vasculature. Finally, most antiangiogenic therapies focus on the inhibition of VEGF and, although the inhibition may be successful, cancer cells may get vascularized through other molecular pathways or even through other vascularization mechanisms, such as vasculogenesis. Several researchers are working on new molecular targets and principles to overcome this problem. For example, [30] shows how the different metabolisms of endothelial cells with respect the remaining cells of the body may be a new target to stop angiogenesis. Other examples include work with microRNAs [31] or immunotherapy combined with antiangiogenic treatments.

3 Mathematical models of tumor-induced angiogenesis

This section reviews the mathematical models that are setting the basis for predictive medicine in cancer. As there is a wide literature regarding tumor-induced angiogenesis modeling, only the most prominent models are shown here. Extensive reviews can be found in [10, 50, 55, 127, 128, 131, 138, 163, 167, 171, 175, 195].

3.1 Classification of the models

Cancer is a multiscale process. It starts with a gene mutation and may spread to other tissues later. Handling every scale is a non-trivial problem for mathematical models and, in many cases, they are limited to one of the following:

- **Subcellular scale**: The characteristic order of magnitude for this scale is nanometers and it includes phenomena such as oncogene transcription, protein creation, signaling cascades, or mutational events.
- **Cellular scale**: The basic unit of this scale is the cell, that is, 10-20 μm. Examples of characteristic phenomena occurring in cancer at this scale are proliferation, apoptosis, cellular communication, and tip endothelial cell migration.
- **Tissue scale**: The order of magnitude of this scale is centimeters and it includes phenomena such as vascular tumor growth, angiogenesis, or adjacent tissue invasion.

In the subsequent review of the literature the models are classified, according to their mathematical abstraction of the biology, into continuous, discrete, and hybrid models. As shown in table 1, each type of model spans different scales. Continuous models are able to describe cancer from a tissue scale, but, in general, cannot track individual cells. Discrete models, on the contrary, are those which track individual cells. These models usually include cellular and subcellular scales, but are not capable of handling the tissue scale, since they are limited by computational power. There are several sub-types of discrete models. The simpler ones are *agent-based models*: Those composed by single units that represent cells which interact among them in a lattice-free space, subjected to certain rules. When the space is subdivided with a lattice and each site can be only occupied by a single cell, the model sub-type is called *cellular automaton*. In this case the cellular shape is not taken into account and it allows the representation of a slightly larger scale. The last discrete sub-type model is the *cellular potts model*, which can be thought as a generalization of the cellular automaton. In the cellular potts model each cell may be composed by several lattice locations or pixels whose states change to minimize a global energy. Finally, hybrid models benefit from the discrete and continuous models advantages, by using both of them. In particular, when there is a single description for each phase they are usually referred to as composite discrete-continuous models. Because the focus of this review is tumor-induced angiogenesis, we classify as hybrid models only those whose treatment of capillaries involve both discrete and continuous descriptions.

3.2 Representative models of tumor-induced angiogenesis

Since the discovery of the critical role of angiogenesis in tumor progression, many researchers have tried to model angiogenesis under different assumptions. One

Table 1 Characteristics of continuous, discrete, and hybrid models

	Continuous models	Discrete models	Hybrid models
Scale	Tissue	Cellular and subcellular	Cellular, subcellular, and tissue
Advantages	Allow to model tumor growth without spatial and temporal limits	Track cells Discrete event description	Combine the advantages of both methods
Disadvantages	Can not track individual cells Can not describe discrete events	Spatially and temporally limited	Greater complexity in the coupling

of the most common is to consider the tumor just as a fixed source of TAF, that is, to model only the growth of capillaries without modeling the tumor. Here we review some notable models, many of which were used afterwards coupled with tumor growth models (as briefly detailed at the end of the section). Relevant angiogenesis models have also been developed for wound healing, as in [145, 198, 199, 201] (see [200] for a review), and for skeletal muscle, as in [43, 123, 165].

3.2.1 Continuous models

One of the first models of angiogenesis was developed by Deakin in 1976 [67]. It was a continuous model consisting of two variables: The endothelial cell density and one chemical species that represented the TAF. Both variables were governed by convection-diffusion equations. Most continuous models coming later, although involving more variables and representing additional phenomena, followed a similar structure. For example, in 1985, Balding and McElwain [14] posed a similar continuum model which also considered one chemical species, but distinguished between tip endothelial cell concentration that migrated chemotactically following the gradient of TAF and stalk endothelial cell concentration that proliferated in the presence of TAF. Furthermore, the model included branching and anastomosis events. A decade later, Byrne and Chaplain [38, 39] extended Balding and McElwain's model by adding TAF consumption and secondary tip proliferation. In the same years, Chaplain and Stuart [57] developed a model that included many essential mechanisms of angiogenesis, which was subsequently simplified in [54] to permit a deeper mathematical analysis. This analysis showed that both endothelial cell proliferation and migration were essential to angiogenesis. Most of these early-stage models were one dimensional.

The next step in continuum models of angiogenesis was the incorporation of haptotaxis; see the work of Orme and Chaplain [56, 148]. In this model, endothelial cells can migrate chemotactically and following a concentration gradient of fibronectin through the ECM. This work studies the importance of haptotaxis versus chemotaxis and the role of fibronectin in haptotaxis. Furthermore, by altering the parameters of the model, they analyze different antiangiogenic strategies. Anderson and Chaplain [8] developed a model to prove an experimental observation: If endothelial cells do not proliferate, angiogenesis does not reach the tumor and it fails to deliver the nourishment. It was a one-dimensional model including chemotaxis and haptotaxis, which was subsequently extended to two dimensions in the first part of [7] and in [53], and to more complex geometries in [197] and in [151]. This model has three variables that represent the concentration of three species: tip endothelial cell, n; fibronectin, f; and a general tumor angiogenic factor, c. The variables are governed by the following partial differential equations:

$$\frac{\partial n}{\partial t} = D_n \Delta n - \nabla \cdot \left(\frac{\chi_0 k_1}{k_1 + c} n \nabla c \right) - \nabla \cdot (\rho_0 n \nabla f) \quad (1)$$

$$\frac{\partial f}{\partial t} = \omega n - \eta n f \quad (2)$$

$$\frac{\partial c}{\partial t} = -\lambda n c \quad (3)$$

where D_n, χ_0, k_1, ρ_0, ω, η, and λ are parameters. The three terms on the right hand side of equation (1) incorporate three different kinds of tip endothelial cell motion: random motility, chemotaxis, and haptotaxis, respectively. Tip endothelial cells also produce and consume fibronection, as modeled by equation (2), and consume tumor angiongenic factor, as modeled by equation (3). The authors performed several simulations in $2\,\text{mm} \times 2\,\text{mm}$ square domains that simulated a piece of corneal tissue. Initially, they placed three tip endothelial cells on the left hand side of the domain, a rightwards decreasing fibronectin gradient, and a rightwards increasing gradient of tumor angiogenic factor. As shown by the time evolution of the tip endothelial cell concentration in figure 7, the tips initially move to the right driven

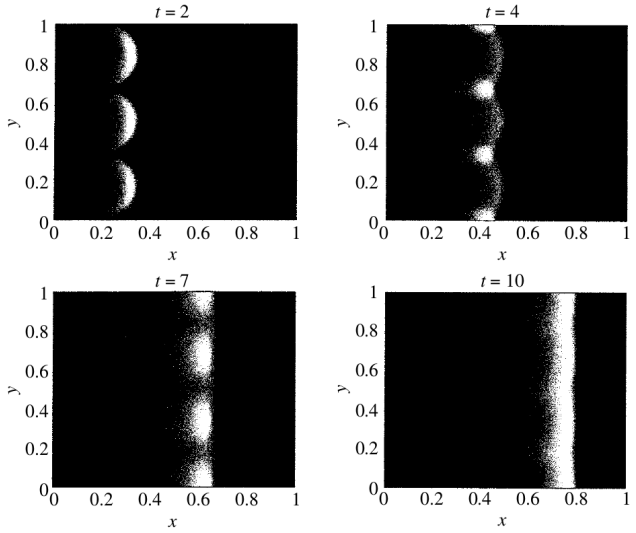

Fig. 7 Numerical solution to equations (1)–(3). Three tip endothelial cells move rightwards, following gradients of tumor angiogenic factor and fibronectin. Reproduced from [7]

by chemotaxis. The effect of haptotaxis and random motion, however, produces a clustering of these cells at later times, that may be interpreted as anastomosis events. This model generated results in qualitative agreement with experiments. Moreover, as shown later in the manuscript, a further development of the model in which the authors discretized equation (1) allowed the representation of the capillaries and the model became widely used.

By 2000, several angiogenesis inhibitors were already well known. Using similar ideas to [7], Anderson *et al.* [9] modeled how secondary tumors remained in dormant states because the already vascularized primary tumor released angiogenic substances that prevented the vascularization of secondary tumors.

Continuous models evolved further to include many other key mechanisms of angiogenesis. For example, Levine and collaborators [118–121] developed models that included endothelial cell migration by chemotaxis (TAF) and haptotaxis (fibronectin), ECM degradation (protease enzyme), and angiogenesis inhibition (angiostatin). Plank *et al.* [156], extended the previous models to include random walks into TEC migration. Some continuum models include mechanochemical interactions between endothelial cells and the extracellular matrix, due to the traction exerted by endothelial cells on ECM fibers when migrating, for instance [97]. Others even consider alternative mechanisms of tumor vascularization, as in [183], where they model vasculogenesis and angiogenesis. One of the latest continuous models was developed by Santos-Oliveira *et al.* [172], which is based in the phase-field method. In this work they model the traction forces exerted by tip endothelial cells and the cell-cell adhesion forces. They study how different responses of other endothelial cells to these forces alter the morphology of incipient sprouts.

Another question which appears when modeling angiogenesis with continuous models is the emplacement of the first endothelial cells, that is, where the activation of angiogenesis starts. In most models, this selection is imposed *a priori* by means of initial conditions. However, some authors endowed their models with different criteria to select those locations. Orme and Chaplain [146] solved this problem taking into account the local accumulation of endothelial cells as the origin of new sprouts. Levine *et al.* [119] addressed the problem by selecting the tip endothelial cell through the interaction of endothelial cells, TAF's, proteases, fibronectin, angiostatin, pericytes, and macrophages. Addison-Smith *et al.* [2] developed a model to predict the origin and spacing between sprouts.

3.2.2 Discrete models

Discrete modeling has also produced quality models to study angiogenesis. Contrary to continuous approaches, these models are able to predict the structure of the new vasculature, allowing comparison with *in vitro* or even *in vivo* experiments. Agent-based models, in general, track TECs which migrate under the influence of a continuum field, while SECs follow their path. One example is the model posed by Stokes and Lauffenburger [186]. It is a lattice-free, two-dimensional model in which every sprout is characterized by its TEC, whose velocity and position is governed by a differential equation (chemotaxis) altered by randomness and viscosity. Furthermore, they include branching ruled by a probability function and anastomosis whenever a tip is away from another endothelial cell a distance equivalent to a cell size. It is noteworthy that the model includes the influence of the redistribution of endothelial cells between the sprout and the parent vessel. Contrary to this detailed description of TECs, the TAF is assumed to be in a steady state. Sleeman and coworkers [154, 155, 181] also developed an agent-based model by getting rid of the lattice of a cellular automata model. In their approach, they model TEC migration as a random walk, in particular, in [155], they used a biased circular random walk [59], based on the work of Hill and Häder [95] for the trajectories of micro-organisms. Sun *et al.* [187] introduced the influence of the extracellular matrix in their agent-based model through an anisotropic directional field that affected tip endothelial cell migration. Using a different approach, Milde and coworkers [137] also modeled the interactions between TECs

and the ECM. Furthermore, their model considered several bounded, cleaved, and soluble VEGFs ([bVEGF], [cVEGF], [sVEGF], respectively), unbound and bound fibronectin ([FIB] and [bFIB], respectively), and metalloproteinases ([MMP]). The description of TECs used an agent-based approach that included migration by chemotaxis (driven by VEGF), haptotaxis (driven by fibronectin), and the influence of the fibers of the ECM whose distribution is supposed to be known. TECs were also endowed with the ability to branch and anastomose with other capillaries. The density of endothelial cells (ρ_e) was approximated each time step through the interpolation of the TEC density ([EC]). The chemical species, on the other hand were governed by the following partial differential equations:

$$\frac{\partial[\text{bVEGF}]}{\partial t} = -v_{bV}[\text{MMP}][\text{bVEGF}] \tag{4}$$

$$\frac{\partial[\text{cVEGF}]}{\partial t} = k_V \Delta[\text{cVEGF}] + v_{bV}[\text{MMP}][\text{bVEGF}] - v_V[\text{cVEGF}]\rho_e - d_V[\text{cVEGF}] \tag{5}$$

$$\frac{\partial[\text{sVEGF}]}{\partial t} = k_V \Delta[\text{sVEGF}] - v_V[\text{sVEGF}]\rho_e - d_V[\text{sVEGF}] \tag{6}$$

$$\frac{\partial[\text{FIB}]}{\partial t} = k_F \Delta[\text{FIB}] + \gamma_F \mathcal{G}\left(F_{\text{th}}, [\text{FIB}]\right)[\text{EC}] - v_{bF}[\text{FIB}](E_\chi bF_{\text{th}} - [\text{bFIB}]) - d_F[\text{FIB}] \tag{7}$$

$$\frac{\partial[\text{bFIB}]}{\partial t} = v_{bF}[\text{FIB}](E_\chi bF_{\text{th}} - [\text{bFIB}]) - \delta_{bF}[\text{bFIB}][\text{MMP}] - d_{bF}[\text{bFIB}] \tag{8}$$

$$\frac{\partial[\text{MMP}]}{\partial t} = k_M \Delta[\text{MMP}] + \gamma_M \mathcal{G}\left(M_{\text{th}}, [\text{MMP}]\right)[\text{EC}] - d_M[\text{MMP}], \tag{9}$$

where $v_\square$, $k_\square$, $d_\square$, M_{th}, F_{th}, bF_{th}, δ_{bF} and γ_F are parameters, $\mathcal{G}(a,b) = (a-b)/a$, and E_χ represent the ECM fibers. Note that the equations for bounded species only present source and sink terms because these species have no mobility. Notably, the authors demonstrated with this model that the structure of the newly created vessels depends on the configuration of the ECM and the level of the different VEGF isoforms.

Capasso *et al.* [42] also included random walks in their model. Yet another example is the three-dimensional model developed by Das *et al.* [65] that includes cell-cell communication and migration as a stochastic process. The work by Bentley and coworkers [28] was a breakthrough in angiogenesis modeling. There, they studied lateral inhibition by means of a hierarchical agent-based model and showed how the feedback loop between VEGF and Dll-4 determined tip or stalk cell differentiation.

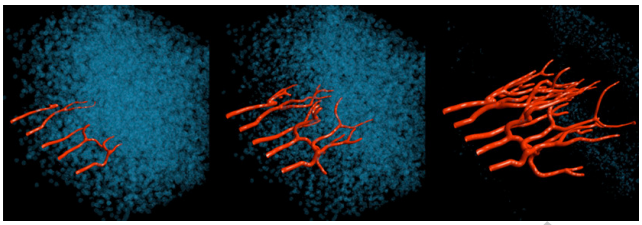

Fig. 8 Three-dimensional discrete agent-based model that includes the interactions between the TECs and the ECM. Reproduced from [137]

One of the most celebrated discrete model was developed by Anderson and Chaplain [7, 52]. They discretized equation (1) of the previously detailed continuous model to create the following cellular automata model:

$$n_{l,m}^{q+1} = n_{l,m}^q P_0 + n_{l+1,m}^q P_1 + n_{l-1,m}^q P_2 + n_{l,m+1}^q P_3 + n_{l,m-1}^q P_4. \tag{10}$$

The probabilities P_i for TEC movement in the cellular automata included diffusion, chemotaxis, and haptotaxis mechanisms, as in the continuous model. Notably, the results were compared with *in vivo* assays performed in the eye of a rabbit [86] and in the cornea of a mouse [140] achieving significant agreement. This idea was a breakthrough because it allowed to represent vascular structures easily. The model was later expanded to three-dimensions, to include different branching and anastomosis criteria, and to model blood flow [51, 134–136, 184, 185]. And, as shown below, many authors use modified versions of this model to simulate vascular tumor growth. In 2005, Kevrekidis and Whitaker [110], using a similar idea, also presented a one-dimensional hybrid model (extended to two dimensions in [111]) that included TAFs, ECM, proteases, and angiogenesis inhibitors.

The cellular potts approaches introduced by Glazier and Graner [89] were also used to model angiogenesis. Bauer *et al.* [17] used such a model, where endothelial cells were able to migrate guided by chemotaxis and haptotaxis. The sprouts were able to branch and anastomose, and the extracellular matrix was modeled in detail. The authors extended the model to study the influence of the ECM in TEC migration [18]. Some other examples of cellular potts models include the work by Mahoney *et al.* [129], where they added haptotaxis to TEC migration, and by Szabó *et al.* [188, 189], where they studied the role of cell-cell adhesion.

Finally, while continuous models have been mostly used to study the process of angiogenesis from a more abstract perspective, discrete modeling has also been applied to more specific experiments. The works that replicate the corneal micropocket angiogenesis assay constitute an important example. The first one was developed

by Tong and Yuan in 2001 [193]. It is a two-dimensional model with an initial circular capillary and a pellet that releases TAF, both embedded in a square domain. New TECs originate at the capillaries stochastically and migrate and anastomose according to discrete rules. This model was extended in [92] to include an angiogenesis inhibitor. Furthermore, in [194] the authors improved the continuous equation that governs the dynamics of TAF. In 2011, Jackson and Zheng [103] proposed a different model for corneal angiogenesis that included a mechanical model for the elongation of the sprouts and angiopoietin-regulated phenotypes.

3.2.3 Hybrid models

Although discrete models can capture the structure of the vascular network, in general, they only describe the migration of TECs and assume that SECs follow their path. In addition, when SECs are modeled, discrete approaches become computationally unaffordable as the number of cells increases. Some authors have developed hybrid models to circumvent these problems. The common approach in hybrid models for angiogenesis is to model TECs using a discrete description, while every other component of the model, such as SECs or TAFs, are modeled as continuum fields. Hence, these models are able to represent the vascular networks, while benefiting from the simplicity and computational effectiveness of continuum modeling. The hybrid model proposed by Travasso and collaborators [70, 196] fits into the latter type of theories. It couples cellular-scale discrete agents with an averaged continuous theory based on the phase field method. The model has shown significant potential predicting *in vivo* patterns of tumor-induced capillary growth (see figure 9). The model by Travasso *et al.* fits into the framework of phase-field theories. In opposition to the classical description of sharp interfaces, the phase-field model describes the interface between phases as diffuse. This permits avoiding the resolution of moving boundary problems, but requires solving a higher-order partial differential equation with diffuse interfaces evolving dynamically over the computational domain. These computational challenges can be easily overcome with appropriate numerical methods, as shown in the next section.

The model has two continuous variables and discrete agents. The first continuous variable, f, represents a balance of TAF, while the second one, c, is an order parameter that defines the location of endothelial cells. The dynamics of these variables are governed by the following reaction-diffusion and phase-field equation

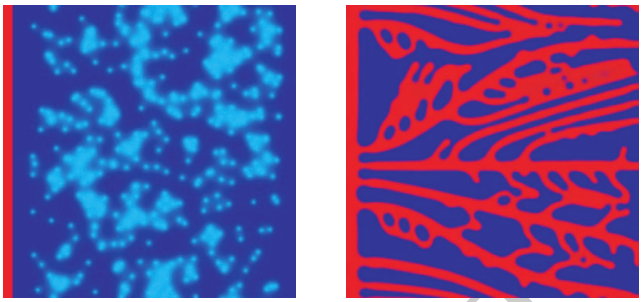

Fig. 9 A hybrid model of tumor-induced angiogenesis. Left: Tumor angiogenic factor (light blue) promotes angiogenesis from an initial vessel (red). Right: The model captures the formation of a new vascular network. Reproduced from [196]

(respectively):

$$\frac{\partial f}{\partial t} = \nabla \cdot (D \nabla f) - B_u f c \mathcal{H}(c) \tag{11}$$

$$\frac{\partial c}{\partial t} = \nabla \cdot \left(M \nabla \left(\mu_c - \lambda^2 \Delta c \right) \right) + \mathcal{B}_p(f)\, c \mathcal{H}(c)\,, \tag{12}$$

where D, B_u, M, and λ are parameters, $\mathcal{H}(\cdot)$ is the Heaviside function, $\mu_c = c(c^2 - 1)$ is the chemical potential, and $\mathcal{B}_p$ is the proliferation function defined by

$$\mathcal{B}_p(f) = \begin{cases} B_p f & \text{if } f < f_p \\ B_p f_p & \text{if } f \geq f_p \end{cases} . \tag{13}$$

Here, B_p is the proliferative rate constant and f_p is the tumor angiogenic factor condition for highest proliferation. Equation (11) accounts for the diffusion and uptake of TAF and equation (12) models the endothelial cell-cell adhesion and stalk cell proliferation in the presence of TAF. TECs are discrete agents in this theory. They are characterized by their center, $\mathbf{x}_{\text{TEC}}$, and radius, R_{TEC}, and are activated when the following rules are met at a point: 1) The point is inside a capillary; 2) the value and gradient of TAF are greater than a threshold; and 3) there is no other TEC in the vicinity of that point (to account for the Delta-Notch selection). TECs are deactivated when at least on of these conditions is not met at the center of the discrete agent. In [196] TEC movement was driven by chemotaxis, such that the TEC velocity was governed by

$$\mathbf{v}_{\text{TEC}} = \chi \nabla f(\mathbf{x}_{\text{TEC}}) \mathcal{L}\left(\|\nabla f(\mathbf{x}_{\text{TEC}})\| \right) \,, \tag{14}$$

where χ is a parameter and $\mathcal{L}(\cdot)$ is a function that limits the maximum velocity of the cell. In latter developments of these theory [203], the authors included a conceptualization of haptotaxis based on circular biased random walks. In their model, the position of TECs was given by,

$$\left.\begin{aligned} x^n_{\text{TEC}} &= x^{n-1}_{\text{TEC}} + \rho \cos(\theta_n) \sin(\varphi_n) \Delta t_n \\ y^n_{\text{TEC}} &= y^{n-1}_{\text{TEC}} + \rho \sin(\theta_n) \sin(\varphi_n) \Delta t_n \\ z^n_{\text{TEC}} &= z^{n-1}_{\text{TEC}} + \rho \cos(\varphi_n) \Delta t_n \end{aligned}\right\} , \tag{15}$$

where n is the current timestep and ρ the velocity magnitude defined as

$$\rho = \chi \left\| \nabla f\left(\mathbf{x}_{\mathrm{TEC}}\right) \right\| \mathcal{L}\left(\left\| \nabla f(\mathbf{x}_{\mathrm{TEC}}) \right\| \right) \ . \tag{16}$$

In equation (15), θ_n and φ_n are realizations of the discrete stochastic variables Θ_n and Φ_n. The latter denote the azimuthal and the polar (zenith) angles of the spherical system of coordinates, respectively, and we assume that they are independent for all $n > 0$. The ranges of Θ_n and Φ_n are defined, respectively, as

$$R_{\Theta_n} = \{\theta_{n-1} + \delta, \theta_{n-1}, \theta_{n-1} - \delta\} \ , \tag{17}$$

$$R_{\Phi_n} = \{\varphi_{n-1} + \delta, \varphi_{n-1}, \varphi_{n-1} - \delta\} . \tag{18}$$

When $n = 1$ equations (17) and (18) can not be straightforwardly applied. In this case, θ_0 and φ_0 should be understood as deterministic values given by the chemotactic direction at the initial time, that is, θ_0^{ch} and φ_0^{ch}. The ranges of Θ_n and Φ_n show that, from one time step to the next and for each angular direction, the tip endothelial cell may remain advancing in the same direction or may turn clockwise or anticlockwise an angle δ. The probabilities of these events are given by the probability functions of Θ_n and Φ_n defined as

$$P\left[\Theta_n = \theta_{n-1} + \delta\right] = \hat{\tau}^{+}_{\theta_n^{\mathrm{ch}}} \Delta t_n \ , \tag{19}$$

$$P\left[\Theta_n = \theta_{n-1} - \delta\right] = \hat{\tau}^{-}_{\theta_n^{\mathrm{ch}}} \Delta t_n \ , \tag{20}$$

$$P\left[\Theta_n = \theta_{n-1}\right] = \left(1 - \hat{\tau}^{+}_{\theta_n^{\mathrm{ch}}} \Delta t_n - \hat{\tau}^{-}_{\theta_n^{\mathrm{ch}}} \Delta t_n\right) \ , \tag{21}$$

$$P\left[\Phi_n = \varphi_{n-1} + \delta\right] = \hat{\tau}^{+}_{\varphi_n^{\mathrm{ch}}} \Delta t_n \ , \tag{22}$$

$$P\left[\Phi_n = \varphi_{n-1} - \delta\right] = \hat{\tau}^{-}_{\varphi_n^{\mathrm{ch}}} \Delta t_n \ , \tag{23}$$

$$P\left[\Phi_n = \varphi_{n-1}\right] = \left(1 - \hat{\tau}^{+}_{\varphi_n^{\mathrm{ch}}} \Delta t_n - \hat{\tau}^{-}_{\varphi_n^{\mathrm{ch}}} \Delta t_n\right) \ , \tag{24}$$

where $\hat{\tau}^{\square}_{\square}$ are the so-called transition rates (see [155]) and θ_n^{ch} and φ_n^{ch} are the azimuthal and polar directions given by the chemotatic direction at time t_n.

Finally, tip endothelial cells must be coupled with the continuous equations of the model. Because they are an endothelial cell phenotype, they are coupled with equation (12). The ratio of the material produced in the tip cell to the volume swept as the cell migrates, gives us the value of the order parameter inside the tip endothelial cell. Thus, in the region of the domain occupied by a tip endothelial cell, the order parameter is given by

$$c_{\mathrm{TEC}} = \frac{4\mathcal{B}_p\left(f\left(\mathbf{x}_{\mathrm{TEC}}\right)\right) R_{\mathrm{TEC}}}{3\rho} . \tag{25}$$

We believe that hybrid models have a significant potential in angiogenesis modeling. As the field evolves and angiogenesis models are coupled with tumor growth theories or additional biological phenomena, hybrid models will prove a very useful tool.

3.2.4 Multiscale models

We believe that significant advances in the field of angiogenesis modeling may be driven in the near future by the integration of several models that operate at different scales. Small-scale models are usually easier to validate because the corresponding experiments are more straightforwardly performed. It would be ideal to use small-scale models to produce data that can be utilized by larger-scale models. Here, we propose an idea to integrate and extend two successful models that operate at different spatial scales, namely, the hybrid model proposed by Travasso *et al.* (see subsection 3.2.3) and the work of Bentley *et al.* [28]. We begin by describing the work of Bentley *et al.* This is a cell-scale model that predicts how TEC selection combines with tip cell migration and fusion. The model accounts for a detailed description of filopodia and may be fed with *in vivo* imaging data. The physics is described by a hierarchical system of agents. In the model, a so-called *cellAgent* is composed by smaller agents called *memAgents*. Figure 10 (top) shows a cellAgent (cylinder) representing one endothelial cell, which is composed by a number of memAgents. MemAgents can be nodes (spheres in the top of figure 10), springs (black lines), or surfaces (four-node squares). The springs represent the cortical tension of the membrane. MemAgents operate autonomously in response to the conditions of the environment. They are allowed to move, so that the membrane's shape can change and the cell can extend filopodia. As the cell's shape changes, new memAgents are created to keep the geometry smooth.

MemAgents have two states; one defines their physical type and another one their filopodia-related location. The state that defines the physical type can be *node*, *spring*, or *surface*. The state describing the filopodia-related location can be set as *none*, *base*, *shaft*, or *top* (see bottom panel of figure 10). To grow a filopodium, a new node and a new spring are created. The leading agent is in state top. When a filopodium spring exceeds the maximum length sL_{max}, a new agent is created in state shaft. As the filopodium grows, new agents in state shaft are created. The changes in memAgents are driven by environmental conditions, in particular, the VEGF concentration.

Bentley *et al.* apply their model to developing mouse retinal vasculature which is sitting upon an astrocytic network; see figure 11. To determine the distribution of VEGF in the environment, the authors note that the VEGF_{165} isoform usually adheres to astrocytes rather than diffusing freely through the ECM. The behavior of VEGF_{165} is in contrast with that of VEGF_{120}, which does not show a preference for astrocytes. Based on

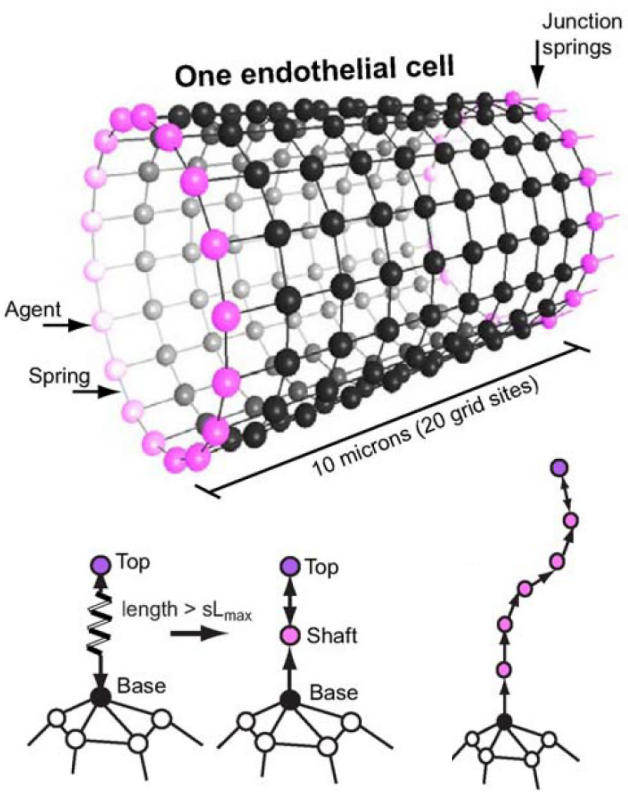

Fig. 10 Model by Bentley *et al.* [28]. Endothelial cell (cylinder in the top panel) represented by a cellAgent. The cellAgent is composed by a number of memAgents, e.g., nodes (solid spheres) and springs (black lines). The whole system constitutes a hierarchy of agents. The nodes of the cellAgent (bottom panel) can be created on the fly and are allowed to move. When the spring is larger that a given threshold sL_{max}, a new node is created. The nodes can take on different states (e.g., base, shaft or top). By moving existing nodes and creating new ones, TECs can extend filopodia. Adapted from [28].

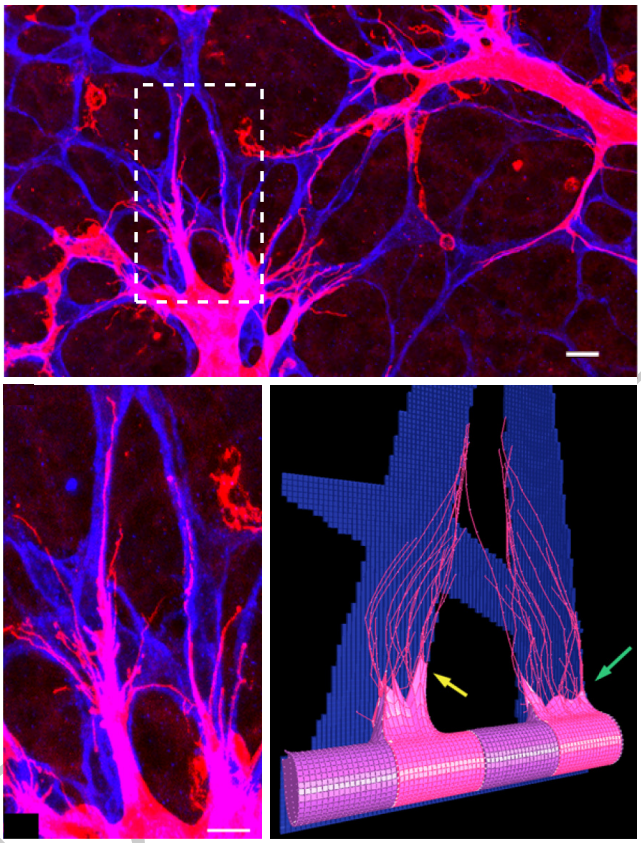

Fig. 11 *In vivo* and *in silico* angiogenesis using Bentley's model [28]. The system corresponds to mouse retinal vasculature. The top panel shows a confocal image of endothelial cells (pink) and astrocytes (blue). The bottom-left panel shows a zoomed in view of the area enclosed by the dashed-line rectangle. Both scale bars represent 10 μm. The bottom-right panel shows a simulation. It is observed that SECs (purple cylinders) remain basically unaltered, while TECs (pink) reshape and develop vigorous filopodia. Adapted from [28].

these observations, the authors model only $VEGF_{165}$ and assume that it is bound to astrocytes.

Figure 11 (top) shows a confocal image of growing vasculature (pink) with profuse filopodia (thin protrusions in pink) and astrocytes (blue). Figure 11 (bottom left) shows a zoomed in view of the experimental image. The bottom right panel shows the corresponding simulation. The plot shows that SECs (purple cylinders) remain almost unaltered, while TECs (pink cells) extend numerous filopodia that follow the paths determined by astrocytes.

We believe that this model could be coupled with that proposed by Travasso *et al.* [196], giving rise to a multiscale model with predictive potential at larger scales. In particular, the TEC compartment of Travasso's model could be replaced with the model of Bentley *et al.* Equation (11) can also be coupled with Bentley's model. The preference of the $VEGF_{165}$ isoform for astrocytes could be modeled using a non-constant diffusion coefficient. Arguably, this would increase the predictive capabilities of the model because the VEGF distribution would not need to be assumed. Bentley's model could also be coupled with a continuous theory for SEC proliferation so that the model could be used at the millimeter scale.

3.2.5 Vascular tumor growth

Although there are still several questions that need to be addressed by angiogenesis models, they have been lately coupled with models for tumor growth. Most of them utilize a discrete description for angiogenesis, as in the work of Frieboes *et al.* [82, 83], which uses discrete random walks to model angiogenesis and phase fields to describe tumor growth. The cellular automata framework and multiscale techniques have also allowed the development of significant models, such as in [4, 150]. Additional important work includes [33, 64, 96, 147, 180, 223]. The hy-

brid angiogenesis model [196] has been recently coupled with tumor growth theories using a ten-species model in [122] and using a phase-field approach in [217, 218].

Fluid transport in the vicinity a tumor, and in particular blood flow through the newly created vessels, has received special attention in mathematical modeling for its important role in tumor growth. Baxter and Jain were among the first to model fluid flow. In the series of papers [19–22] they studied transport of fluid and molecules in one- and two-dimensional settings and addressed the role of fluid pressure in tumor growth. Pries, Secomb, and collaborators worked on the role of blood flow in vascular networks, including the adaptation of vessels to the flow conditions [158–162, 178]. Most of the subsequent models that included blood flow used their theory. As an example, they recently developed a mathematical model [177] that coupled the discrete angiogenesis model of Tong and Yuan [193] with their models of blood flow and vascular adaptation. Rieger and coworkers developed a two-dimensional cellular automata model [16] (which was extended to three-dimensions in [116]) that considered both tumor growth and angiogenesis and included vessel co-option, vessel collapse, and cell death. Notably, vessels collapse and regress due to absence of intravascular blood flow. In [207] the authors incorporated details from the cellular automata model in [4] and analyzed the distribution of a drug injected into the vasculature. Posterior developments of this model [208–210] included more realistic arterio-venous initial vascular networks and interstitial fluid pressure to study the influence in tumor growth. Phipps and Kohandel also studied interstitial fluid pressure within a continuous angiogenesis model [152]. In [213, 214], Wu and coworkers built intravascular and extravascular fluid pressure into an augmented version of the angiogenesis model developed in [7]. They used the model in [162] for the intravascular flow and the work in [19] for the extravascular flow. Later, in [40] they coupled this model with a tumor growth model based on the work in [6]. Wu *et al.* followed a similar approach in [215], but they also incorporated the effect of the lymphatic system.

4 Simulation of tumor angiogenesis

The first mathematical models of tumor-induced angiogenesis generally focused on the growth of new capillary sprouts at a small scale, and were usually simulated in simplistic one- or two-dimensional setups. Their role was crucial to understand the biology and physics behind angiogenesis and they set the basis for future mathematical models of this problem. Newer models, in many instances built upon the previous, have been developed to include a wider range of phenomena. Furthermore, many of these models are simulated nowadays in experimental setups, which are more complex but rise the possibility of quantitative comparison with *in vivo* situations. We are now at the point where new computational challenges arise as a result of the increased complexity, geometries, and quantitation of the simulations. These challenges need to be overcome to make the models predictive.

One of the first computational challenges that emerges is the need to perform full-scale, three-dimensional simulations in relevant geometries. This is a general challenge of angiogenesis modeling because virtually all approaches include continuous equations. Furthermore, some theories involve higher-order derivatives that need a special treatment, such as those in [83, 93, 196, 211]. At present, there are a number of numerical methods that can deal with each of these challenges separately, but only a few can handle all of them in a robust and accurate way. One of the most promising algorithms is isogeometric analysis (IGA) [99], that permits an efficient solution of high-order equations being at the same time geometrically flexible and accurate.

Another challenge of angiogenesis modeling is the need to feed the models with *in vitro* or, even better, *in vivo* data. Furthermore, the inherent uncertainty in the parameters needs to be considered. We refer the reader to the recent review by Oden *et al.* [144] that deals with this topic in the context of tumor growth. Additionally, in order to mimic either experiments or patient-specific setups, the initial conditions and geometries need to be replicated in the simulations. The fast development of imaging techniques in the last years has allowed the characterization of the vessels in the tumor micro-environment with enough resolution to capture capillaries. These data, which usually come in the form of pixels or voxels, need to be incorporated in the simulations. Those models that rely on continuous equations for the capillaries can include them in an almost direct fashion. Conversely, the data needs to be pre-processed for discrete models. In the former case, phase-field modeling stands out over the rest, as its quasi-binary order parameter easily accommodates the way in which imaging data is provided. In the latter case, the pre-processing method usually consists in obtaining the middle lines or skeletons of the capillaries.

4.1 Isogeometric analysis

IGA is a generalization of finite element analysis (FEA, [98]) whose initial goal was to unify computer-aided design (CAD) and FEA. The main idea of this method is to replace the FEA traditional basis functions with those

utilized in CAD, such as B-splines, non-uniform rational B-splines (NURBS) [153, 166], T-splines [26, 48], hierarchical B-splines [173, 176], trimmed NURBS [174], polynomial splines over hierarchical T-meshes (PHT-splines) [142], Powell-Sabin B-splines [182], or rational Triangular Bézier Splines [216]. IGA invokes the isoparametric concept, that is, the unknown variables are represented in terms of the same basis functions which define the geometry. The coefficients of the basis functions are the degrees of freedom or control variables. IGA is a nascent technology compared with the long tradition behind FEA, and, consequently, it still presents some topics that are being addressed, such as optimized quadrature rules [13, 101] or the creation of solid volumes from surfaces. The growing community behind IGA is currently dealing with these topics, which, in any case, are not directly related with the simulation of angiogenesis.

Because IGA uses the CAD description of the geometry it benefits from the naturally built-in geometric flexibility and the high-order continuity of the basis functions. Moreover, IGA also excels in its high-order accuracy, robustness, and compact support. For these reasons, IGA has been successfully used in several fields such as fluid mechanics [3, 23, 73], phase-field models [34, 35, 68, 69, 88, 124, 125], structural vibrations [62, 100], shell modeling [27, 112], contact problems [66, 71, 72], fluid-structure interaction [24, 25, 47], shape optimization [204], electromagnetics [36], and cardiovascular applications [11, 25, 139]. Also, several groups have developed open-source software for IGA, such as, PetIGA [60], igatools [149], or GeoPDEs [74].

In the following, we briefly describe the concept of B-splines and NURBS and we show a NURBS-based IGA example based on the Galerkin discretization for the hybrid tumor-induced angiogenesis model described in section 3. Note, however, that IGA is not restricted to the Galerkin method and has been used with other discretizations such as the collocation method [12, 49, 164] or the least-squares finite element method [108].

4.1.1 B-splines and NURBS

For the construction of a B-spline basis we need a knot vector, that is, a non-decreasing set of coordinates in the parameter space[2]. Let $\Xi = \{\xi_1, \xi_2, \ldots, \xi_{n+p+1}\}$ be the knot vector[3], where $\xi_i \in \mathbb{R}$ is the ith knot, i is the knot index, $i = 1, 2, \ldots, n+p+1$, $n \in \mathbb{N}$ is the number of basis functions, and p the polynomial order or degree. A univariate B-spline basis, $N_{i,p}$, is defined recursively starting with piece-wise constants ($p = 0$):

$$N_{i,0}(\xi) \begin{cases} 1 & \text{if } \xi_i \leq \xi < \xi_{i+1}, \\ 0 & \text{otherwise.} \end{cases} \tag{26}$$

For higher degrees $p = 1, 2, \ldots$ the basis is defined using the Cox-de Bor recursion formula:

$$N_{i,p}(\xi) = \frac{\xi - \xi_i}{\xi_{i+p} - \xi_i} N_{i,p-1}(\xi) + \frac{\xi_{i+p+1} - \xi}{\xi_{i+p+1} - \xi_{i+1}} N_{i+1,p-1}(\xi). \tag{27}$$

Figure 12a shows an example for $p = 2$. Note that the support of each basis function consists of $p + 1$ *knot spans*.

B-spline curves $\mathbf{C}(\xi)$ in $\mathbb{R}^d$, where d is the number of spatial dimensions, are constructed by taking a linear combination of n B-spline basis as follows:

$$\mathbf{C}(\xi) = \sum_{i=1}^{n} \mathbf{B}_i N_{i,p}(\xi), \tag{28}$$

where $\mathbf{B}_i \in \mathbb{R}^d$ is a vector of coefficients referred to as control points. p-degree B-splines are $\mathcal{C}^{p-1-m}$-continuous across knot spans, where m is the multiplicity of the knot, and $\mathcal{C}^\infty$-continuous elsewhere. As an example, figure 12b shows a two-dimensional B-spline where $p = 2$ and $\Xi = [0, 0, 0, 1, 1, 3, 4, 5, 5, 5]$. Note that the fourth knot value is repeated twice, so the continuity there is $\mathcal{C}^0$.

Using the notion of tensor products, these concepts can be easily generalized to multiple dimensions. Let d_p be the number of parametric directions; for each parametric direction $\ell = 1, \ldots, d_p$ we define a knot vector Ξ^ℓ, such that,

$$\Xi^\ell = \left\{\xi_1^\ell, \xi_2^\ell, \ldots, \xi_{n_\ell + p_\ell + 1}^\ell\right\}, \tag{29}$$

where p_ℓ and n_ℓ are the polynomial order and the number of basis functions for each parametric direction, respectively. We also define a multi-index $\mathbf{i} \in \mathbb{Z}^{d_p}$, the set

$$I = \left\{\mathbf{i} = \{i_1, \ldots, i_{d_p}\} \mid i_\ell \in \{1, \ldots, n_\ell\},\ \ell = 1, \ldots, d_p\right\}, \tag{30}$$

and a multi-index of polynomial orders $\mathbf{p} = \{p_1, p_2, \ldots, p_{d_p}\}$. Given a control net $\{\mathbf{B_i}\}$ a multivariate B-spline is defined by

$$\mathbf{V}(\boldsymbol{\xi}) = \sum_{\mathbf{i} \in I} \mathbf{B_i} N_{\mathbf{i},\mathbf{p}}(\boldsymbol{\xi}), \tag{31}$$

where, using a tensor product structure, the multivariate basis function $N_{\mathbf{i},\mathbf{p}}(\boldsymbol{\xi})$ is defined as

$$N_{\mathbf{i},\mathbf{p}}(\boldsymbol{\xi}) = \prod_{\ell=1}^{d_p} N_{i_\ell,p_\ell}^\ell\left(\xi^\ell\right). \tag{32}$$

[2] Knots partition the parameter space into elements.

[3] The standard in CAD are open knot vectors, defined as those whose first and last knot values appear $p + 1$ times.

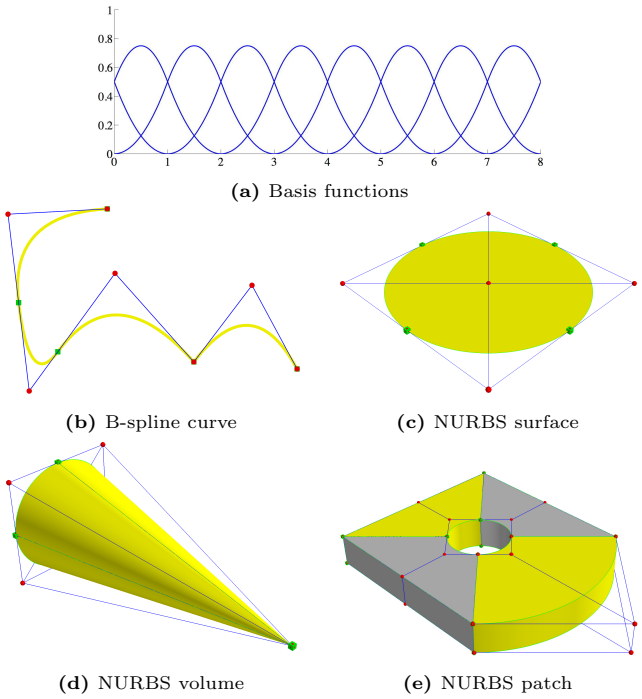

(a) Basis functions

(b) B-spline curve **(c)** NURBS surface

(d) NURBS volume **(e)** NURBS patch

Fig. 12 Basis functions, B-splines, and NURBS. Control points are drawn as red dots, knots as green squares, control nets as blue lines, and knot spans as green lines

Non-uniform rational B-splines (NURBS) are a generalization of B-splines. $\mathbb{R}^d$ NURBS are obtained from the projection of $\mathbb{R}^{d+1}$ B-splines and they allow the exact representation of several useful geometries, such as conics. Given $\mathbf{i}$ and $\mathbf{p}$, the basis of a B-spline can be projected to create a basis of NURBS in the following way:

$$R_{\mathbf{i},\mathbf{p}}\left(\boldsymbol{\xi}\right) = \frac{w_{\mathbf{i}} N_{\mathbf{i},\mathbf{p}}\left(\boldsymbol{\xi}\right)}{\sum_{\mathbf{j}\in I} w_{\mathbf{j}} N_{\mathbf{j},\mathbf{p}}\left(\boldsymbol{\xi}\right)}, \tag{33}$$

where $w_{\mathbf{i}}$ are positive constants referred to as weights. Similarly to B-splines, NURBS curves, surfaces, and volumes are created by the linear combination of a control mesh and their piece-wise basis functions as

$$\mathbf{V}\left(\boldsymbol{\xi}\right) = \sum_{i\in I} \mathbf{B}_{\mathbf{i}} R_{\mathbf{i},\mathbf{p}}\left(\boldsymbol{\xi}\right). \tag{34}$$

Figure 12c shows the exact parametrization of a conic section, and figure 12d shows a cone built with NURBS. More complex geometries are constructed using two or more NURBS patches, that is, the union of NURBS, as shown in figure 12e. NURBS and B-splines can also be refined using three different strategies: knot insertion (classical h-refinement), order elevation (classical p-refinement), and k-refinement, which increases smoothness in addition to order.

4.1.2 NURBS-based isogeometric analysis and the Galerkin method

Here, we show an example of IGA discretization using NURBS and the Galerkin method. We will use the hybrid model first presented in [196] and extended to account for haptotaxis in three dimensions in [203]. This model includes several of the computational challenges mentioned at the beginning of the section: it is a three-dimensional problem that involves cellular and tissue scales in addition to higher-order derivatives. By using the proposed discretization the simulations can be easily performed in realistic geometries, as shown in [218]. Note also that the model includes discrete agents. The agents are coupled with the continuous equations as shown in [202].

We begin by considering a weak form of the continuous equations (11) and (12). Without loss of generality, we assume free-flux boundary conditions at this point. Let $\mathcal{V}$ denote the trial solution and the weighting function spaces, which are assumed to be the same. The space $\mathcal{V}$ is a subset of $\mathcal{H}^2$, the Sobolev space of square integrable functions with square integrable first and second derivatives. By multiplying equations (11) and (12) with smooth functions, integrating over the domain, and applying integration by parts we derive the variational formulation. The problem may be stated as follows: find $f, c \in \mathcal{V}$ such that $\forall w_1, w_2 \in \mathcal{V}$:

$$\int_\Omega w_1 \frac{\partial f}{\partial t} d\Omega + \int_\Omega \nabla w_1 D \nabla f d\Omega + \int_\Omega w_1 B_u f c \mathcal{H}\left(c\right) d\Omega = 0 \tag{35}$$

$$\int_\Omega w_2 \frac{\partial c}{\partial t} d\Omega + \int_\Omega \nabla w_2 M \nabla \mu_c \, d\Omega + \int_\Omega \Delta w_2 M \lambda^2 \Delta c \, d\Omega - \int_\Omega w_2 \mathcal{B}_p\left(f\right) c \mathcal{H}\left(c\right) d\Omega = 0 \tag{36}$$

We make use of the Galerkin method to perform the spatial discretization. Let us define the discrete space $\mathcal{V}^h$, which is a subset of $\mathcal{V}$. We approximate equations (35) and (36) by the following variational problem over the finite dimensional space: find $f^h, c^h \in \mathcal{V}^h \subset \mathcal{V}$ such that $\forall w_1^h, w_2^h \in \mathcal{V}^h \subset \mathcal{V}$:

$$\int_\Omega w_1^h \frac{\partial f^h}{\partial t} d\Omega + \int_\Omega \nabla w_1^h D \nabla f^h d\Omega + \int_\Omega w_1^h B_u f^h c^h \mathcal{H}\left(c^h\right) d\Omega = 0 \tag{37}$$

$$\int_\Omega w_2^h \frac{\partial c^h}{\partial t} d\Omega + \int_\Omega \nabla w_2^h M \nabla \mu(c^h) d\Omega + \int_\Omega \Delta w_2^h M \lambda^2 \Delta c^h d\Omega - \int_\Omega w_2^h \mathcal{B}_p\left(f^h\right) c^h \mathcal{H}\left(c^h\right) d\Omega = 0 \quad (38)$$

Here, f^h is defined as

$$f^h(\mathbf{x}, t) = \sum_{A=1}^{n_b} f_A(t) N_A(\mathbf{x}) \quad (39)$$

where n_b is the dimension of the discrete space $\mathcal{V}^h$ and the coefficients f_A are the control variables and N_A are the basis functions. Since we will use a conforming discretization, the relation $\mathcal{V}^h \subset \mathcal{V}$ holds and the discrete functions are required to be in $\mathcal{H}^2$. This condition is satisfied by the globally $\mathcal{C}^1$-continuous second order basis functions. The rest of the variables of equations (37) and (38), namely c^h, w_1^h, and w_2^h, are defined analogously to f^h.

4.2 Neo-vasculature structure quantification

A significant computational challenge is to perform quantitative comparisons and validations against experiments and predictions of the simulations. In the literature we find several methods to make direct quantitative measures; some examples include averaged cell density, vessel lengths, or diameters [61, 179, 193]. There are also indirect measures of the vasculature, such as the oxygen distribution within the region of interest [132]. These methods, however, do not capture the faulty structure of tumor-induced capillaries, which, as shown in subsection 2.2.4, is responsible for the defective blood transport of these vessels. We think that these measures are essential to validate angiogenesis models and we outline a method to extract these features of the vessel structure in the following.

The idea is that a vascular network can be reduced to a graph $G = (V, E)$, which is defined as a nonempty set of vertices $V = \{v_i\}$ and a set of edges $E = \{e_j\}$, where each edge is a pair of vertices $e_j = (v_a, v_b)$. In our case, the vertices are the branching points of the capillaries and the edges the capillaries themselves. Then, using graph theory one can select specific graph descriptors that contain information of the topology, connectivity, or other relevant features of the structure of the vascular network. The descriptors are able to quantify not only the static configuration, but also the evolution of the network, being thus a valuable tool to study the dynamics of the angiogenic model.

The definition of the graph that characterizes a simple capillary network may be done by hand. For example at the beginning of a two-dimensional simulation there may be just a dozen of new capillaries, whose vertices and edges can be manually identified. The connection of the vertices with the edges and the final extraction of its graph takes an affordable time, and the risk of error is low. However, as the simulation evolves, the network develops and the amount of capillaries grows quickly. The growth is even faster in three-dimensional networks, and an automated process is needed.

For these reasons, one of the pillars of this methodology is the techniques and algorithms that lead to an automatic graph extraction, namely *binarization*, *skeletonization*, and *graph identification*. Roughly speaking, the methodology to extract the graph from a suitable image consists in the following: The first technique is the binarization, whose objective is to transform the image of interest into a binary image, such that the vascular network is clearly identified (with value one) and other non-interesting features in the image are eliminated (value zero). Then, the binary image is transformed until only a one-point-thin, body-centered curve or *skeleton* remains (see [169] for a review of different methods of the topic). Finally, a graph identification algorithm is applied to the skeletonized image. This technique mainly consists in the identification of the components of the graph from the skeleton, that is the branching points of the skeleton as vertices V and the branches as edges E. The extraction of the graph ends with the definition of a matrix, namely the *A-matrix*, from which the descriptors of the graph can be evaluated.

This methodology could be applied almost straightforwardly to both *in vivo* and *in vitro* images obtained by different techniques such as magnetic resonance (MR) or intravital microscopy [106]. The only difference would be in the binarization algorithm: the image should be treated with suitable filters in order to obtain a binary image to which the skeletonization can be applied.

The application of the described methodology to *in vivo* and *in vitro* angiogenesis images provides a quantification of the vascular network that could be used to validate the model.

5 Results

In this section we present some numerical results of the hybrid model discretized above that exemplifies the computational challenges of section 4. We begin by considering an analysis of the model presented in [196] in two dimensions to show its features and the biological phenomena included in this theory. Next, we illustrate

the neo-vasculature quantification through a comparison with the model presented in [203] that includes haptotaxis. Finally, we exploit several features of IGA to overcome some of the computational challenges outlined above, which allow us to perform accurate three-dimensional simulations.

5.1 Analysis of the model

In this section we analyze the hybrid model presented in [196]. The analysis is performed through two-dimensional simulations rather than three-dimensional, as in the latter case the study of the results becomes difficult due to the tangled vessel patterns. For the first example we have chosen an academic setting that has been frequently used in the literature: a square tissue with a tumor and a straight capillary along one of the edges. In particular, in this numerical example, the domain is $\overline{\Omega} = [0, 300]^2$, which represents a tissue of 375 µm × 375 µm. We use a uniform mesh with 256^2 knot spans and quadratic basis functions with $\mathcal{C}^1$-continuity across element boundaries. We employ free flux boundary conditions in the vertical direction and periodic conditions in the horizontal direction. The tumor is represented by 200 randomly-distributed hypoxic cells. A 37.5 µm wide vessel is located at the bottom. Figure 13a shows this configuration, where we used the following color code (which is maintained throughout the paper): red color for capillaries and green color for tumor angiogenic factor.

Figure 13 shows snapshots of the solution at different times. At the beginning of the simulation, the 200 hypoxic cells start to release tumor angiogenic factor, which diffuses throughout the domain (figure 13b). Once the factor reaches the initial vessel at the bottom of the domain, with enough concentration to activate a tip endothelial cell, angiogenesis is initiated. In figure 13c we observe that one tip endothelial cell has become active and has started its migration. At this moment, there is only one tip cell because the cell itself prevents the activation of further TECs in its close vicinity by means of the lateral inhibition mechanism. Meanwhile, the other cells stimulated by the tumor angiogenic factor attain a proliferative phenotype, generating an incipient capillary behind the tip endothelial cell. Proliferation results in a consumption of the tumor angiogenic factor that becomes more evident in figure 13d. As the leading cell moves away from the initial vessel, new tip endothelial cells get activated, because the lateral inhibition mechanism does not affect them anymore. The vessel network continues growing and new sprouts appear forming branches (figures 13e and 13f). The growth and branching proceeds (figures 13g to 13i) until all the hypoxic cells become normoxic. This process creates a tortuous and defective vascular pattern characteristic of tumor angiogenesis; see figure 13j.

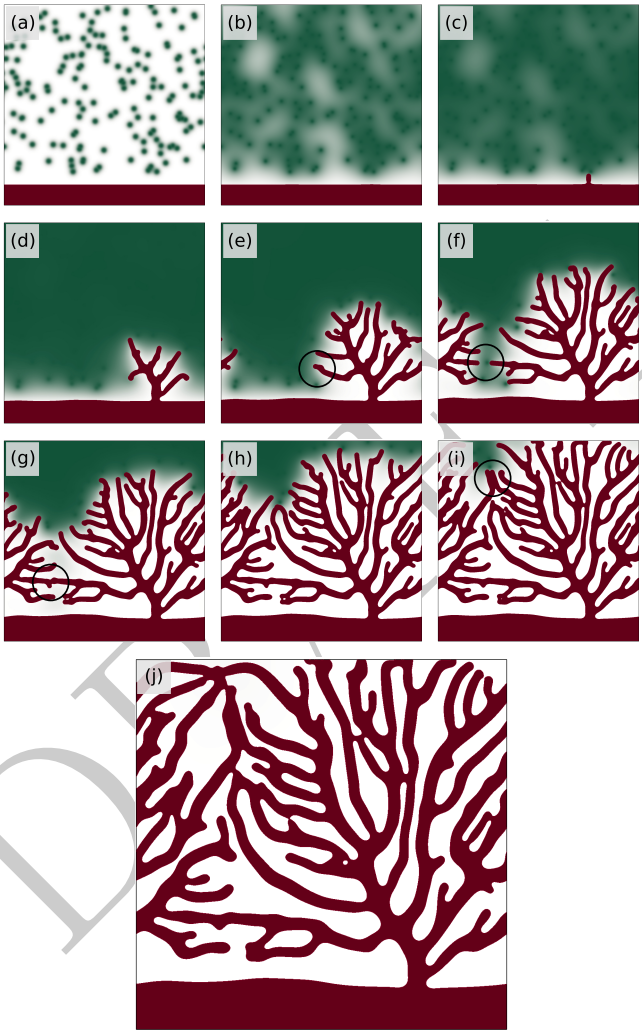

Fig. 13 Formation of a vascular network. Two hundred randomly-distributed hypoxic cells release tumor angiogenic factor (in green) that triggers angiogenesis from a pre-existing capillary (in red). New capillaries leaded by tip endothelial cells grow and form a new vascular network. In their growth, they consume angiogenic factor and anastomose with other capillaries. The resulting vascular pattern presents a defective structure characteristic of tumor-induced angiogenic vessel networks

Through the simulation we can study the movement of tip endothelial cells. In this particular model, only chemotaxis orchestrates the migration, that is, cells move towards hypoxic cells following the gradients of tumor angiogenic factor. As endothelial cells approach the location of hypoxic cells, the latter become normoxic and the release of tumor angiogenic factor ceases. However, if the tip cell is not deactivated, it becomes attracted toward neighboring hypoxic cells, creating turns in the

growing capillaries, as shown in figure 13e. During the simulation, tip endothelial cells may find other endothelial cells in their migration direction. In these cases (see details in figures 13f and 13g) they merge one with another originating anastomoses. However, in the simulation, anastomosis events only take place when two tip cells concur at the location of a hypoxic cell. If other biological phenomena such as haptotaxis or filopodia detection were included in the model, anastomosis events would be more frequent and not determined by the location of hypoxic cells. For example, the highlighted region of figure 13i shows two capillaries that run parallel and very close. In this situation, the leading cells of the capillaries should have detected each other by means of filopodia, anastomosed, and formed a loop.

In the next set of examples, shown in figure 14, we study the influence of the initial location of the capillaries and distribution of hypoxic cells. The figure presents the initial condition (top row) and an advanced stage of the development of the new vasculature (bottom row) of four simulations. These examples, although still theoretical and not directly based on experiments, aim at reflecting more realistic situations to analyze the model. To this end, we start by replicating the simulation of figure 13 in a bigger domain (figure 14, first column): a square $\overline{\Omega} = [0, 700]^2$ that represents a tissue of 875 µm × 875 µm. Its surface is approximately 5.4 times larger than that of the previous example; however, we use the same mesh: 256^2 knot spans. Even with this coarse mesh, we are able to capture the sharp interfaces created in the phase field. Through this simple example we illustrate the capabilities of isogeometric analysis to overcome computational challenges, such as the need for high accuracy methods. From the qualitative comparison of figure 13 and the left column of figure 14 we may conclude that the final patterns hold similar characteristics, even at different scales, regarding the tree-like structure, the width of capillaries, the number of branches, and the density of the pattern. Note that, again, because the model only includes chemotaxis, the number of anastomosis events is low and most of them are located at the position of hypoxic cells. In addition, as highlighted in the left-hand side plots of the figure, TECs get deactivated even in the proximity of other capillaries.

With the goal of moving towards more realistic examples, we present a simulation in the second column of figure 14 with the same distribution of two hundred hypoxic cells, but with an altered configuration of the initial capillaries. Instead of geometric shapes, we create a setup that is closer to an initial vascular network in a real tissue. The resulting pattern is formed by two main tree-like structures, connected at two points. The first structure grows from the left initial capillary and spans the majority of the domain. Conversely, the second network, which starts from the topmost initial vessel, is smaller because its development started later. Note how the vessels span the regions of the domain with hypoxic cells. For example, the top left region is not invaded by the neovasculature, as it was free of hypoxic cells.

In the next simulation (third column in the figure), we choose a circular initial capillary surrounding a similar random distribution of hypoxic cells. We select this configuration for its similitude with the mouse corneal micropocket angiogenesis assay [109, 140], one of the most used *in vivo* experiments. The blood vessels located at the corneal limbus would be represented by the circular capillary and the space inside would be the avascular cornea seeded with cancer cells mimicked by hypoxic cells. Note that this configuration could also be compared with the dorsal skin chamber experiment (see [106]) with no previous capillaries, in which a tumor is implanted and angiogenesis may be easily observed through intravital microscopy. The final network of this simulation is formed by three main structures grown from the circular capillary. The structures have branched and fused with one another through anastomosis. Additionally, there are three other minor structures and, on the bottom region, we observe an incipient capillary that eventually stopped growing due to the absence of tumor angiogenic factor.

Finally, as presented in the rightmost column of figure 14, we focus on the distribution of hypoxic cells. Four capillaries are located in a simplistic configuration, each of them in one edge of the square domain. Conversely, we distribute the hypoxic cells in a more complex and realistic fashion. They follow four normal density functions with the mean located at different points of the tissue. This initial configuration represents a multifocal tumor, such as those observed *in vivo* at early stages of cancer development, or an heterogeneous tumor in which only some groups of clonal expansions are able to promote angiogenesis. The pattern shown at the bottom row, demonstrates two facts. First, if hypoxic cells are not close enough to the initial capillary, angiogenesis does not start. Such situation occurs in the top and right foci. Second, the model is able to generate vascular networks that span each foci.

5.2 Quantitation

In this section we show an example of the method to quantify the structure of vasculature created by the angiogenesis model. The method is outlined in figure 15. There, we compare the final pattern of two 2D simulations with identical initial conditions, boundary condi-

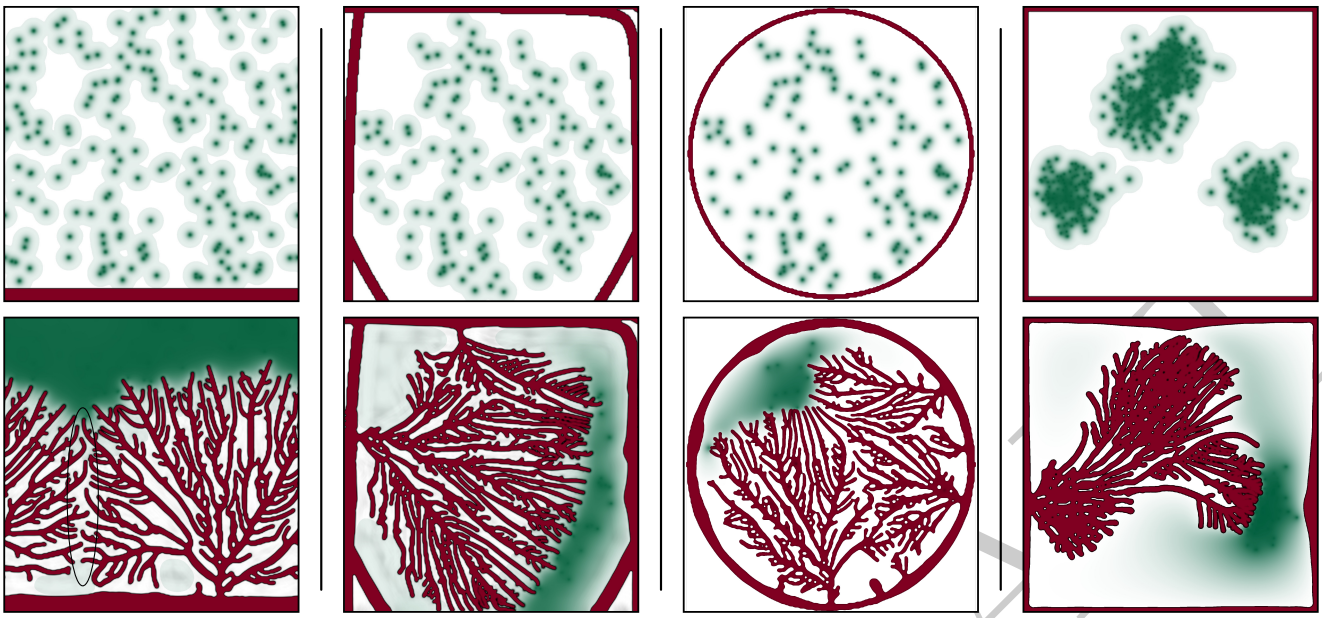

Fig. 14 Influence of initial conditions in a bigger domain. Initial conditions (top) and advanced stage of angiogenesis (bottom) of four simulations. The domain represents a 875 µm × 875 µm tissue. The first three simulations start with the same random distribution of hypoxic cells, but their difference in the initial capillaries promotes distinct vasculatures. The multifocal distribution of hypoxic cells in the last simulation generates a vascular network that spans every foci

tions, and parameters, but using different mathematical models. The first (in gray) only includes chemotaxis, while the second (in red), includes both chemotaxis and haptotaxis. Note that the simulation without haptotaxis is the final pattern of the numerical example in figure 13. When the two final patterns defined by the phase-field are qualitatively compared, as in figure 15a, it is clear that, although both vasculatures span the domain and oxygenate the tissue, they are different. The superimposed images on the right-hand side of this figure show that the only characteristic shared by the patterns is that both were initiated from the same point in the parent vessel. This was predictable, as the criteria for the activation are equal. Besides this point (and the beginning of the branch that starts there), both vasculatures differ; there is not a single branch that follows the same path in both simulations.

In order to make a quantitative comparison we developed a numerical method to extract the graphs associated to vascular networks. This numerical method is divided into two parts. The first one is to transform a discretized binary image of the phase-field that represents the capillaries into a skeleton, that is, a one-point-wide, body-centered curve topologically equivalent to the vascular network (see figure 15b). To obtain the skeleton, we use a two-fold-iteration parallel thinning algorithm based on [222]. As this algorithm does not ensure the skeleton to be one-point wide, we designed a sequential thinning algorithm that we apply to the previous skeleton to guarantee this property. The second part of the method is to define a distance-weighted simple graph from the skeleton. This is done by means of an algorithm that identifies the vertices and edges in the skeleton and assigns a distance to the edges (used as weights). From the resulting weighted graph (figure 15c) we can define and study quantities of interest to compare the vasculatures generated by both models.

The first remarkable observation is that the representation of the skeletons in figure 15b already reveals distinguishing characteristics of the networks that were not clear in the phase-field representation. The skeleton of the simulation that includes haptotaxis shows a lattice-like structure compared to the tree-like structure of the purely chemotatic simulation. This fact is even more apparent when we prune the branches of the skeleton that do not form loops (represented in light gray and red). These branches are those capillaries that do not allow blood flow because they do not form loops, so they barely contribute to tissue oxygenation. In addition, we observe that the reason for the lattice-like structure is that the branches of the skeleton do not run parallel to each other due to the haptotaxis conceptualization incorporated in this model. Anastomosis events occur more frequently in the model with haptotaxis because the chemotactic direction is altered, which favors the formation of loops.

The quantitative measurements of the extracted graphs shown in figure 15c backup all these observations and

(a) Comparison of the phase fields. The superimposed image on the right-hand side shows that haptotaxis completely alters the vascular patterns

(b) Skeletonization of the phase fields. The increased anastomosis in the simulation with haptotaxis changes the skeleton to a lattice-like structure

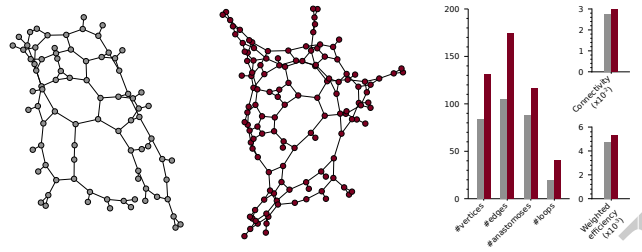

(c) Skeletons are transformed into distance-weighted graphs to quantify the vascular networks. Note the increased connectivity and efficiency when haptotaxis is present

Fig. 15 Quantitative comparison of two simulations without and with haptotaxis. Two simulations are compared, one using the model without haptotaxis (in gray) and one using the model with haptotaxis. The comparison exemplifies a quantitative method to extract measures of the structure of a vascular network

add useful indices to compare the vasculatures. The graph of the model with haptotaxis presents a higher number of vertices and edges, that is, the model promotes more branching and anastomosis events. Furthermore, the average edge length is lower (10.31 versus 16.19 for the purely chemotactic) and the algebraic connectivity [78] is higher, distinctive of a more lattice-like network. The graph of the haptotactic model has over twice the number of loops of the other (41 versus 20). We also analyzed the distance-weighted efficiency of the network, defined as

$$E = \frac{1}{n\,(n-1)} \sum_{i,j\in[1,n],i\neq j} \frac{1}{d\,(i,j)}\ , \tag{40}$$

where n is the number of vertices and $d\,(i,j)$ is the distance of the shortest path between vertices i and j. The efficiency measures the traffic capacity of the network and reflects its parallel transfer ability [63]. In our case, it represents the ability of the network to transport oxygen and nutrients to the tissue. The graph associated to the haptotactic model has greater efficiency according to this metric. We see how by means of this method one can retrieve quantitative indices to extract features of the networks useful to characterize the new vessels networks.

5.3 Three-dimensional angiogenesis

The hybrid mathematical model developed in [203] gathers several computational challenges: it includes cellular and tissue scales, includes higher-order derivatives, and is a fully three-dimensional theory. Here, we simulate this model to show how isogeometric analysis allows to overcome these challenges.

For every simulation in this section we use a computational domain $\overline{\Omega} = [0, 300]^3$, which represents a cube with side length 375 µm. We use a uniform mesh defined by the tensor product of open knot vectors and quadratic basis functions. Each knot vector is composed by 72 knot spans. Note this mesh is coarser than those used in the previous examples. In particular, the side of the knot spans is almost 3.5 times larger than in the first simulation of section 5. Still, IGA permits to accurately simulate the mathematical model using this mesh. As in previous examples, we impose no-flux boundary conditions in all directions but one, in which we assume periodicity. This direction, as in previous simulations, is the direction parallel to the axis of the initial capillaries, so that we allow the capillaries to transverse this boundary and potentially create more complex patterns.

Firstly, we perform two simulations as shown in figures 16 and 17. There, we present several snapshots of the dynamics of angiogenesis stimulated by different configurations of hypoxic cell clusters. The first snapshot of each figure represents the initial conditions. Both simulations start with two 25 µm wide rectilinear capillaries that transverse the cube parallel to each other. The capillaries are located so that every cell within the tissue represented by the computational domain is less than 220 µm away from a blood vessel, that is, the tissue is initially well oxygenated. However, as tumor cells require higher amounts of oxygen and nutrients, we place hypoxic cells in the domain. The difference between both simulations stems from the number and distribution of hypoxic cells. In the first simulation (figure 16), 200 hypoxic cells are distributed following a normal distribution centered in the cube, so that they mimic a dense tumor. In the second simulation (figure 17), 300 hypoxic cells are grouped in three clusters, as in a multifocal tumor. These configurations favor the initiation of angiogenesis from both capillaries and thus potentially

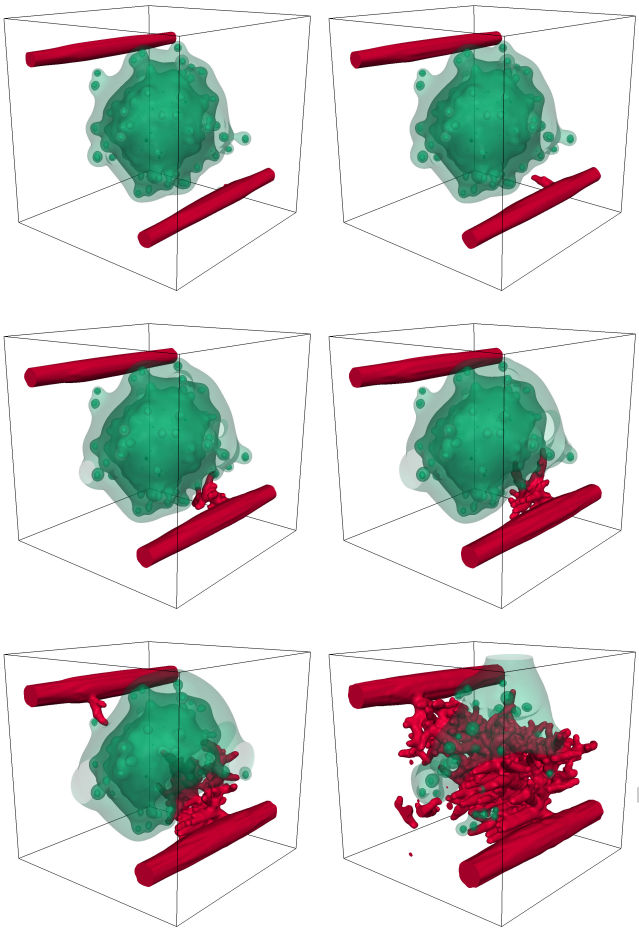

Fig. 16 Three-dimensional angiogenesis simulation from two parent capillaries. Angiogenesis is triggered by the tumor angiogenic factor (green isosurfaces) released from hypoxic cells disposed forming a tumor-like structure. The tip endothelial cells that lead the growth of the sprouts migrate by chemotaxis and haptotaxis. A new vascular network develops from two parent capillaries and pervades the tumor, leaving no cells under hypoxic conditions. The initial capillaries get connected through the new network allowing the blood to flow between them. The simulation is performed on the cubic domain $\overline{\Omega} = [0, 300]^3$

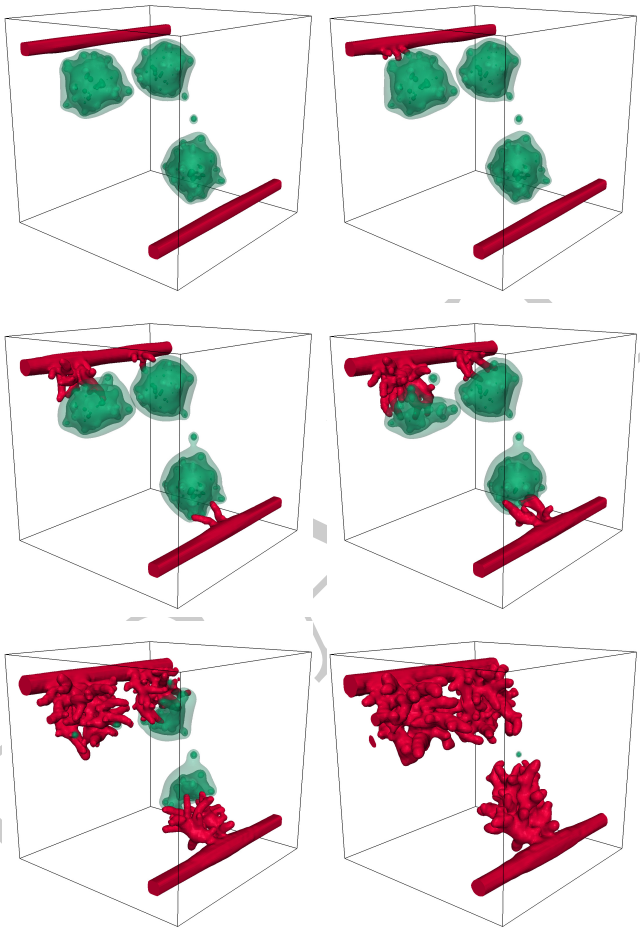

Fig. 17 A multifocal tumor promotes angiogenesis in three-dimensions. Three cluster of hypoxic cells that mimic a multifocal tumor trigger the creation of a new vascular network. The resulting vasculature forms three structures that satisfy the oxygen demands of the clusters, but that are independent and not connected to each other

allow the connection between the initial vessels through the new vasculature.

In the first simulation (figure 16), the tumor angiogenic factor (green isosurfaces) released by the cluster of hypoxic cells diffuses until it reaches the initial capillaries. At that moment angiogenesis is triggered, but initially only from the bottom blood vessel. Meanwhile, the growth factor produces the enlargement of the upper capillary, which may be interpreted as vasodilatation. The new network initiated from the bottom continues growing, partially oxygenating the tumor in its way. Finally, the tumor angiogenic factor promotes the growth of new capillaries from the upper initial vessel which branch and pervade the tumor from the other side. Towards the end of the simulation, several anastomosis events connect both structures, allowing the blood to flow between the two initial capillaries. Note that in three dimensions the probability of anastomoses events is significantly lower than in two dimensions. At this point, the majority of the tumor is normoxic; only scattered hypoxic regions remain which will eventually get oxygenated. The simulation ends when there is no tumor angiogenic factor left in the domain, that is, when all the tumor is pervaded by the new network.

The second simulation (figure 17) evolves in a similar fashion. However, the initial distribution of hypoxic cells in three clusters promotes a different network spread. Angiogenesis starts from three different regions in this simulation; two in the upper capillary and one in the bottom one. Each region is located in the close vicinity

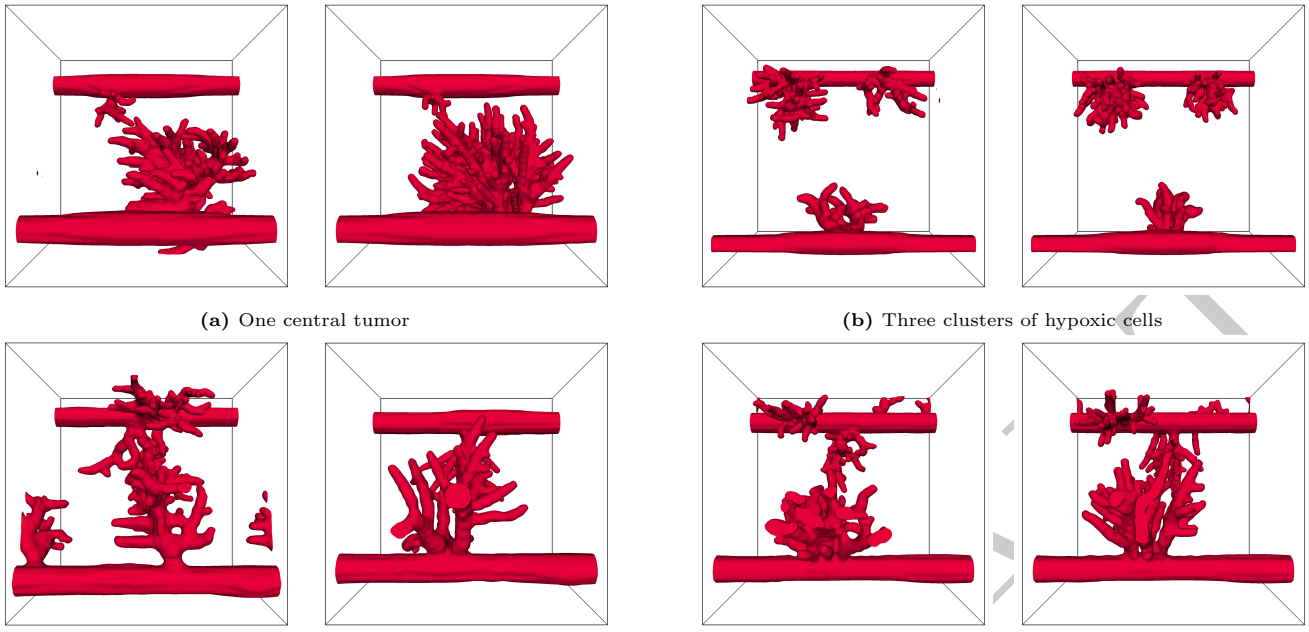

(a) One central tumor

(b) Three clusters of hypoxic cells

(c) One hundred randomly distributed hypoxic cells

(d) Two hundred randomly distributed hypoxic cells

Fig. 18 Influence of haptotaxis in angiogenesis. Each subfigure shows the final pattern produced by the model with haptotaxis (left) and the model without haptotaxis (right). Every simulation starts with two initial capillaries parallel to each other. We detail in each caption the initial condition of the hypoxic cells. Note that the left snapshots of figures 18a and 18b correspond to figures 16 and 17, respectively. The patterns of the vasculatures for each model differ in tortuosity, number of anastomosis events (connectivity), and length of the capillaries

of each hypoxic cluster and because these cells are at a similar distance to the initial capillary, angiogenesis starts from the three regions almost at the same time when compared with the previous simulation. This simulation shows a plain example of the role of haptotaxis in the migration of tip endothelial cells. In the third snapshot of the figure two capillaries are growing from the bottom initial vessel. However, while one of them is led by a tip cell that migrates directly towards the center of the tumor, the other one is, at this point, surrounding it. The migration of the leading cell of the latter capillary has been altered by the biased circular random walk and moves away from its otherwise purely chemotactic direction. Haptotaxis, however, acts only on the small scales, as shown in the next snapshot where the tip cell has already recovered the chemotactic direction and turns again towards the cluster of hypoxic cells. By the end of the simulation, the multifocal tumor has promoted the creation of three vascular networks. Contrary to the previous simulation, these networks remain unconnected and thus, blood cannot flow between the initial capillaries.

Figure 18 shows an analysis of the role of haptotaxis in three dimensions. We show an advanced time stage of the development of the vascular networks of four pairs of simulations. In each subfigure, the snapshot on the left-hand side was produced by the model with chemotaxis and haptotaxis, while that on the right-hand side was generated under exactly the same conditions, but with the model that only considers chemotaxis. The initial condition for the capillaries is shared for every simulation: two straight capillaries parallel to each other. The initial conditions for the hypoxic cells, conversely, are different for each pair of simulations. Thus, figures 18a and 18b correspond to the previous simulations presented in figures 16 and 17, respectively; the vasculature in figure 18c is initiated with 100 randomly distributed hypoxic cells; and the vasculature in figure 18d is initiated with 200 randomly distributed hypoxic cells.

We observe that the growth patterns generated by each model are dissimilar in various aspects. The most prominent difference is the greater tortuosity of the capillaries generated by the model with haptotaxis, closer to that observed in experiments. In this theory (see left-hand side snapshots), although the global migration of tip cells is governed by chemotaxis, we observe how tip endothelial cells turn away by means of haptotaxis and reorient towards the hypoxic cells. This phenomenon, although working at small scales, alters significantly the final patterns which envelop the tumor. Conversely, in the right-hand side snapshots, tip endothelial cells go directly towards the source of growth factor generating

straighter capillaries. We also observe a higher number of anastomosis events in the patterns shown on left-hand side, mainly produced by tip cells that deviate from the chemotatic direction and encounter in their path other endothelial cells. This leads to a another difference between the morphology of the vasculatures: capillaries are shorter in the model with haptotaxis, as anastomosis stops their growth more frequently.

Isogeometric analysis permitted us to perform the simulations presented in this section and to analyze two models in three-dimensional setups. By altering the initial conditions, we simulated several possible capillary and tumor arrangements and obtained, as a result, a variety of final vascular patterns richer than those presented in previous sections. The simulations suggest that, for mathematical models to achieve the topological complexity observed in *in vivo* angiogenesis experiments, two-dimensional simulations may not be enough. We also believe that the accurate modeling of anastomosis, a crucial process in tumor angiogenesis, may require full-scale three-dimensional simulation.

6 Discussion

"All models are wrong but some are useful" is a celebrated quote by George Box [32] that we abide to. The complexity of tumor-induced angiogenesis makes it very difficult to derive a theory with predictive capabilities in a wide range of situations. We believe that significant progress in tumor angiogenesis research can be made by deriving models that aim at understanding particular mechanisms in simple, but concrete experimental setups. We hope this manuscript provides a starting point to move in this direction and to derive useful models that respond to relevant biological questions. A potential example of this is the model outlined in section 3.2.4. Another interesting development would be to study models with several tumor angiogenic factors. Perhaps even more important would be to account for pro- and anti-angiogenic substances in the theory. The idea of using a local excitator and a global inhibitor is ubiquitous in biology and has led to fundamental insights, e.g., in cellular migration [168]. Another area that deserves attention is vascular remodeling, in particular the understanding of capillary regression and regrowth, which is crucially important in tumor dynamics.

Computational modeling will not establish itself firmly in tumor angiogenesis research unless the models are rigorously validated with experimental data. We expect that inversion methods, Bayesian statistics, and machine learning will play a significant role in this endeavor. We also advocate the method based on graph theory that we propose in the manuscript. This method provides important quantitative information about vascular networks. The approach is also useful to couple angiogenesis models with blood flow simulations because there are reliable 1D methods to compute blood flow that account for the complicated rheology of blood at small scales [178]. We would also like to emphasize the critical role of efficient numerical methods. Simulations of tumor angiogenesis have been performed too often on two-dimensional square domains. This assumption completely ignores the geometrical conditions of the experiment and leads to a dramatic loss of predictive power.

We feel that parameter estimation is also a key challenge. Our vision is that successful models will include an algorithm to compute the parameters in an automated and personalized manner [220]. In our opinion, this process will involve high-resolution medical imaging. The combination of computational methods and imaging is very natural, especially when the model is based on phase fields. The intensity field of an image can also be thought of as a phase field, which provides a straightforward path to the coupling of the technologies. Moore's law seems to be flattening out in computer's processing power, but it is clearly at work in medical imaging. The opportunity is too good to miss.

Acknowledgements The authors gratefully acknowledge the support from the European Research Council, Xunta de Galicia, Consellería de Cultura, Educación e Ordenación Universitaria, Ministerio de Economía y Competitividad, and FEDER.

Compliance with Ethical Standards

Conflict of Interest The authors declare that they have no conflict of interest.

Funding GV and HG were partially supported by the European Research Council (contract #307201), Xunta de Galicia, and by Ministerio de Economía y Competitividad (contract #DPI-2013-44406-R, cofinanced with FEDER funds). IC was partially supported by Consellería de Cultura, Educación e Ordenación Universitaria of the Xunta de Galicia (grant #GRC2014/039).

References

1. URL https://euroliv.files.wordpress.com/2014/05/tumores.jpg
2. Addison-Smith, B., McElwain, D.L.S., Maini, P.K.: A simple mechanistic model of sprout spacing in tumour-associated angiogenesis. Journal of Theoretical Biology **250**(1), 1 – 15 (2008). doi:10.1016/j.jtbi.2007.08.030. URL http://www.sciencedirect.com/science/article/pii/S0022519307003979

3. Akkerman, I., Bazilevs, Y., Kees, C.E., Farthing, M.W.: Isogeometric analysis of free-surface flow. Journal of Computational Physics **230**(11), 4137–4152 (2011). doi:10.1016/j.jcp.2010.11.044. URL http://www.sciencedirect.com/science/article/pii/S0021999110006595
4. Alarcón, T., Byrne, H.M., Maini, P.K.: A cellular automaton model for tumour growth in inhomogeneous environment. Journal of Theoretical Biology **225**(2), 257–274 (2003). doi:10.1016/S0022-5193(03)00244-3
5. Alberts, B., Johnson, A., Lewis, J., Raff, M., Roberts, K., Walter, P.: Molecular biology of the cell. Garland Science (2007)
6. Anderson, A.R.A.: A hybrid mathematical model of solid tumour invasion: the importance of cell adhesion. Mathematical Medicine and Biology **22**(2), 163–186 (2005). doi:10.1093/imammb/dqi005
7. Anderson, A.R.A., Chaplain, M.A.J.: Continuous and discrete mathematical models of tumor-induced angiogenesis. Bulletin of Mathematical Biology **60**(5), 857–899 (1998). doi:10.1006/bulm.1998.0042
8. Anderson, A.R.A., Chaplain, M.A.J.: A mathematical model for capillary network formation in the absence of endothelial cell proliferation. Applied Mathematics Letters **11**(3), 109–114 (1998). doi:10.1016/S0893-9659(98)00041-X
9. Anderson, A.R.A., Chaplain, M.A.J., García-Reimbert, C., Vargas, C.A.: A gradient-driven mathematical model of antiangiogenesis. Mathematical and Computer Modelling **32**(10), 1141–1152 (2000). doi:10.1016/S0895-7177(00)00196-5
10. Araujo, R.P., McElwain, D.L.S.: A history of the study of solid tumour growth: The contribution of mathematical modelling. Bulletin of Mathematical Biology **66**(5), 1039–1091 (2004). doi:10.1016/j.bulm.2003.11.002
11. Auricchio, F., Conti, M., Ferraro, M., Morganti, S., Reali, A., Taylor, R.L.: Innovative and efficient stent flexibility simulations based on isogeometric analysis. Computer Methods in Applied Mechanics and Engineering **295**, 347–361 (2015). doi:10.1016/j.cma.2015.07.011. URL http://www.sciencedirect.com/science/article/pii/S0045782515002236
12. Auricchio, F., Beirão da Veiga, L., Hughes, T.J.R., Reali, A., Sangalli, G.: Isogeometric collocation methods. Mathematical Models and Methods in Applied Sciences **20**(11), 2075–2107 (2010). doi:10.1142/S0218202510004878. URL http://www.worldscientific.com/doi/abs/10.1142/S0218202510004878
13. Auricchio, F., Beirão da Veiga, L., Hughes, T.J.R., Reali, A., Sangalli, G.: Isogeometric collocation for elastostatics and explicit dynamics. Computer Methods in Applied Mechanics and Engineering **249-252**, 2–14 (2012). doi:10.1016/j.cma.2012.03.026. URL http://www.sciencedirect.com/science/article/pii/S0045782512001028
14. Balding, D., McElwain, D.L.S.: A mathematical model of tumour-induced capillary growth. Journal of Theoretical Biology **114**(1), 53–73 (1985). doi:10.1016/S0022-5193(85)80255-1
15. Baluk, P., Hashizume, H., McDonald, D.M.: Cellular abnormalities of blood vessels as targets in cancer. Current Opinion in Genetics & Development **15**(1), 102–111 (2005). doi:10.1016/j.gde.2004.12.005. URL http://www.sciencedirect.com/science/article/pii/S0959437X04001911
16. Bartha, K., Rieger, H.: Vascular network remodeling via vessel cooption, regression and growth in tumors. Journal of Theoretical Biology **241**(4), 903–918 (2006). doi:10.1016/j.jtbi.2006.01.022. URL http://dx.doi.org/10.1016/j.jtbi.2006.01.022
17. Bauer, A.L., Jackson, T.L., Jiang, Y.: A cell-based model exhibiting branching and anastomosis during tumor-induced angiogenesis. Biophysical Journal **92**(9), 3105–3121 (2007). doi:10.1529/biophysj.106.101501
18. Bauer, A.L., Jackson, T.L., Jiang, Y.: Topography of extracellular matrix mediates vascular morphogenesis and migration speeds in angiogenesis. PLoS Computational Biology **5**(7), e1000,445 (2009). doi:10.1371/journal.pcbi.1000445. URL http://dx.doi.org/10.1371%2Fjournal.pcbi.1000445
19. Baxter, L.T., Jain, R.K.: Transport of fluid and macromolecules in tumors I. Role of interstitial pressure and convection. Microvascular Research **37**(1), 77–104 (1989). doi:10.1016/0026-2862(89)90074-5
20. Baxter, L.T., Jain, R.K.: Transport of fluid and macromolecules in tumors II. Role of heterogeneous perfusion and lymphatics. Microvascular Research **4**(2), 246–263 (1990). doi:10.1016/0026-2862(90)90023-K
21. Baxter, L.T., Jain, R.K.: Transport of fluid and macromolecules in tumors III. Role of binding and metabolism. Microvascular Research **41**(1), 5–23 (1991). doi:10.1016/0026-2862(91)90003-T
22. Baxter, L.T., Jain, R.K.: Transport of fluid and macromolecules in tumors IV. A micro-

scopic model of the perivascular distribution. Microvascular Research **41**(2), 252–272 (1991). doi:10.1016/0026-2862(91)90026-8

23. Bazilevs, Y., Calo, V.M., Cottrell, J.A., Hughes, T.J.R., Reali, A., Scovazzi, G.: Variational multiscale residual-based turbulence modeling for large eddy simulation of incompressible flows. Computer Methods in Applied Mechanics and Engineering **197**(1-4), 173–201 (2007). doi:10.1016/j.cma.2007.07.016. URL http://www.sciencedirect.com/science/article/pii/S0045782507003027
24. Bazilevs, Y., Calo, V.M., Hughes, T.J.R., Zhang, Y.: Isogeometric fluid-structure interaction: Theory, algorithms, and computations. Computational Mechanics **43**(1), 3–37 (2008). doi:10.1007/s00466-008-0315-x
25. Bazilevs, Y., Calo, V.M., Zhang, Y., Hughes, T.J.R.: Isogeometric fluid–structure interaction analysis with applications to arterial blood flow. Computational Mechanics **38**(4-5), 310–322 (2006). doi:10.1007/s00466-006-0084-3
26. Bazilevs, Y., Michler, C., Calo, V.M., Hughes, T.J.R.: Isogeometric variational multiscale modeling of wall-bounded turbulent flows with weakly enforced boundary conditions on unstretched meshes. Computer Methods in Applied Mechanics and Engineering **199**(13-16), 780–790 (2010). doi:10.1016/j.cma.2008.11.020
27. Benson, D.J., Bazilevs, Y., Hsu, M.C., Hughes, T.J.R.: Isogeometric shell analysis: The Reissner–Mindlin shell. Computer Methods in Applied Mechanics and Engineering **199**(5-8), 276–289 (2010). doi:10.1016/j.cma.2009.05.011. URL http://www.sciencedirect.com/science/article/pii/S0045782509001820
28. Bentley, K., Mariggi, G., Gerhardt, H., Bates, P.A.: Tipping the balance: Robustness of tip cell selection, migration and fusion in angiogenesis. PLoS Computational Biology **5**(10), e1000,549 (2009). doi:10.1371/journal.pcbi.1000549
29. Bergers, G., Benjamin, L.E.: Tumorigenesis and the angiogenic switch. Nature Reviews Cancer **3**(6), 401–410 (2003). doi:10.1038/nrc1093. URL http://www.nature.com/nrc/journal/v3/n6/full/nrc1093.html
30. Bock, K.D., Georgiadou, M., Carmeliet, P.: Role of endothelial cell metabolism in vessel sprouting. Cell Metabolism **18**(5), 634 – 647 (2013). doi:10.1016/j.cmet.2013.08.001. URL http://www.sciencedirect.com/science/article/pii/S1550413113003252
31. Boon, R.A., Dimmeler, S.: MicroRNAs in myocardial infarction. Nature Reviews Cardiology **12**(3), 135–142 (2015). doi:10.1038/nrcardio.2014.207. URL http://dx.doi.org/10.1038/nrcardio.2014.207
32. Box, G.E.: Robustness in the strategy of scientific model building. Robustness in statistics **1**, 201–236 (1979). doi:10.1016/B978-0-12-438150-6.50018-2
33. Breward, C.J.W., Byrne, H.M., Lewis, C.E.: A multiphase model describing vascular tumour growth. Bulletin of Mathematical Biology **65**(4), 609–640 (2004). doi:10.1016/S0092-8240(03)00027-2
34. Bueno, J., Bona-Casas, C., Bazilevs, Y., Gomez, H.: Interaction of complex fluids and solids: theory, algorithms and application to phase-change-driven implosion. Computational Mechanics **55**(6), 1105–1118 (2015). doi:10.1007/s00466-014-1098-x. URL http://dx.doi.org/10.1007/s00466-014-1098-x
35. Bueno, J., Starodumov, I., Gomez, H., Galenko, P., Alexandrov, D.: Three dimensional structures predicted by the modified phase field crystal equation. Computational Materials Science **111**, 310 – 312 (2016). doi:10.1016/j.commatsci.2015.09.038. URL http://www.sciencedirect.com/science/article/pii/S0927025615006199
36. Buffa, A., Sangalli, G., Vázquez, R.: Isogeometric analysis in electromagnetics: B-splines approximation. Computer Methods in Applied Mechanics and Engineering **199**(17-20), 1143–1152 (2010). doi:10.1016/j.cma.2009.12.002
37. Burri, P.H., Hlushchuk, R., Djonov, V.: Intussusceptive angiogenesis: its emergence, its characteristics, and its significance. Developmental Dynamics **231**(3), 474–488 (2004). doi:10.1002/dvdy.20184. URL http://dx.doi.org/10.1002/dvdy.20184
38. Byrne, H.M., Chaplain, M.A.J.: Mathematical models for tumour angiogenesis: Numerical simulations and nonlinear wave solutions. Bulletin of Mathematical Biology **57**(3), 461–486 (1995). doi:10.1016/S0092-8240(05)81778-1
39. Byrne, H.M., Chaplain, M.A.J.: Explicit solutions of a simplified model of capillary sprout growth during tumor angiogenesis. Applied Mathematics Letters **9**(1), 69–74 (1996). doi:10.1016/0893-9659(95)00069-3. URL http://www.sciencedirect.com/science/article/pii/0893965995000693
40. Cai, Y., Wu, J., Xu, S., Long, Q., Yao, W.: Numerical simulation of inhibiting effects on solid tumour cells in anti-angiogenic therapy: application of coupled mathematical model of angiogenesis with tumour growth. Applied Mathematics and

Mechanics - English Edition **32**(10), 1287–1296 (2011). doi:10.1007/s10483-011-1500-9. URL http://dx.doi.org/10.1007/s10483-011-1500-9

41. Camidge, D.R., Jodrell, D.I.: Introduction to the Cellular and Molecular Biology of Cancer, chap. Chemotherapy, pp. 399–413. Oxford University Press Inc. (2005)
42. Capasso, V., Morale, D.: Stochastic modelling of tumour-induced angiogenesis. Journal of Mathematical Biology **58**(1-2), 219–233 (2009). doi:10.1007/s00285-008-0193-z. URL http://dx.doi.org/10.1007/s00285-008-0193-z
43. Carlier, A., Geris, L., Bentley, K., Carmeliet, G., Carmeliet, P., Van Oosterwyck, H.: MOSAIC: A multiscale model of osteogenesis and sprouting angiogenesis with lateral inhibition of endothelial cells. PLoS Computational Biology **8**(10), e1002,724 (2012). doi:10.1371/journal.pcbi.1002724. URL http://dx.doi.org/10.1371%2Fjournal.pcbi.1002724
44. Carmeliet, P.: Angiogenesis in life, disease and medicine. Nature **438**(7070), 932–936 (2005). doi:10.1038/nature04478. URL http://dx.doi.org/10.1038/nature04478
45. Carmeliet, P., Jain, R.K.: Angiogenesis in cancer and other diseases. Nature **407**(6801), 249–257 (2000). doi:10.1038/35025220. URL http://www.nature.com/nature/journal/v407/n6801/full/407249a0.html
46. Carmeliet, P., Jain, R.K.: Molecular mechanisms and clinical applications of angiogenesis. Nature **473**(7347), 298–307 (2011). doi:10.1038/nature10144. URL http://dx.doi.org/10.1038/nature10144
47. Casquero, H., Bona-Casas, C., Gomez, H.: A NURBS-based immersed methodology for fluid-structure interaction. Computer Methods in Applied Mechanics and Engineering **284**, 943–970 (2015). doi:10.1016/j.cma.2014.10.055
48. Casquero, H., Lei, L., Bona-Casas, C., Zhang, J., Gomez, H.: A hybrid variational-collocation immersed method for fluid-structure interaction using unstructured T-splines. International Journal for Numerical Methods in Engineering **105**(11), 855–880 (2015). doi:10.1002/nme.5004
49. Casquero, H., Lei, L., Zhang, J., Reali, A., Gomez, H.: Isogeometric collocation using analysis-suitable T-splines of arbitrary degree. Computer Methods in Applied Mechanics and Engineering **301**, 164–186 (2016). doi:10.1016/j.cma.2015.12.014. URL http://www.sciencedirect.com/science/article/pii/S004578251500420X
50. Chaplain, M.A.J.: Avascular growth, angiogenesis and vascular growth in solid tumours: The mathematical modelling of the stages of tumour development. Mathematical and Computer Modelling **23**(6), 47–87 (1996). doi:10.1016/0895-7177(96)00019-2. URL http://www.sciencedirect.com/science/article/pii/0895717796000192
51. Chaplain, M.A.J.: Mathematical modelling of angiogenesis. Journal of Neuro-Oncology **50**(1-2), 37–51 (2000). doi:10.1023/A:1006446020377
52. Chaplain, M.A.J., Anderson, A.R.A.: Mathematical modelling, simulation and prediction of tumour-induced angiogenesis. Invasion Metastasis **16**(4-5), 222–234 (1996). URL http://europepmc.org/abstract/MED/9311387
53. Chaplain, M.A.J., Anderson, A.R.A.: On Growth and Form: Spatio-Temporal Pattern Formation in Biology, chap. Modeling the growth and form of capillary networks., pp. 225–249. Wiley (1999). URL http://eu.wiley.com/WileyCDA/WileyTitle/productCd-0471984515.html
54. Chaplain, M.A.J., Giles, S.M., Sleeman, B.D., Jarvis, R.J.: A mathematical analysis of a model for tumour angiogenesis. Journal of Mathematical Biology **33**(7), 744–770 (1995). doi:10.1007/BF00184647. URL http://www.scopus.com/inward/record.url?eid=2-s2.0-0029198056&partnerID=40&md5=afbb11e8485fb1509a8ff13d57da2b74
55. Chaplain, M.A.J., McDougall, S.R., Anderson, A.R.A.: Mathematical modeling of tumor-induced angiogenesis. Annual Review of Biomedical Engineering **8**, 233–257 (2006). doi:10.1146/annurev.bioeng.8.061505.095807
56. Chaplain, M.A.J., Orme, M.E.: Vascular Morphogenesis: In vivo, in vitro, in mente, chap. Mathematical modeling of tumor-induced angiogenesis, pp. 205–240. Birkhauser Boston (1998). doi:10.1007/978-1-4612-4156-0_15
57. Chaplain, M.A.J., Stuart, A.M.: A model mechanism for the chemotactic response of endothelial cells to tumour angiogenesis factor. IMA Journal of Mathematics Applied in Medicine and Biology **10**(3), 149–168 (1993). doi:10.1093/imammb/10.3.149. URL http://www.scopus.com/inward/record.url?eid=2-s2.0-0027761692&partnerID=40&md5=ceb0061096871dd9b656a97cac0e7de5
58. Chauviere, A.H., Hatzikirou, H., Lowengrub, J.S., Frieboes, H.B., Thompson, A.M., Cristini, V.: Mathematical oncology: How are the mathematical and physical sciences contributing to the war

on breast cancer? Current Breast Cancer Reports **2**(3), 121–129 (2010). doi:10.1007/s12609-010-0020-6. URL http://www.ncbi.nlm.nih.gov/pmc/articles/PMC2987530/

59. Codling, E.A., Plank, M.J., Benhamou, S.: Random walk models in biology. Journal of The Royal Society Interface **5**(25), 813–834 (2008). doi:10.1098/rsif.2008.0014
60. Collier, N., Dalcin, L., Calo, V.M.: PetIGA: High-performance isogeometric analysis (2013). URL https://bitbucket.org/dalcinl/petiga
61. Connor, A.J., Nowak, R.P., Lorenzon, E., Thomas, M., Herting, F., Hoert, S., Quaiser, T., Shochat, E., Pitt-Francis, J., Cooper, J., Maini, P.K., Byrne, H.M.: An integrated approach to quantitative modelling in angiogenesis research. Journal of The Royal Society Interface **12**(110) (2015). doi:10.1098/rsif.2015.0546
62. Cottrell, J.A., Reali, A., Bazilevs, Y., Hughes, T.J.R.: Isogeometric analysis of structural vibrations. Computer Methods in Applied Mechanics and Engineering **195**(41-43), 5257–5296 (2006). doi:10.1016/j.cma.2005.09.027. URL http://www.sciencedirect.com/science/article/pii/S0045782505005451
63. Criado, R., del Amo, A.G., Hernández-Bermejo, B., Romance, M.: New results on computable efficiency and its stability for complex networks. Journal of Computational and Applied Mathematics **192**(1), 59 – 74 (2006). doi:10.1016/j.cam.2005.04.051. URL http://www.sciencedirect.com/science/article/pii/S0377042705003080
64. Cristini, V., Lowengrub, J.S., Nie, Q.: Nonlinear simulation of tumor growth. Journal of Mathematical Biology **46**(3), 191–224 (2003). doi:10.1007/s00285-002-0174-6
65. Das, A., Lauffenburger, D., Asada, H., Kamm, R.D.: A hybrid continuum-discrete modelling approach to predict and control angiogenesis: Analysis of combinatorial growth factor and matrix effects on vessel-sprouting morphology. Philosophical Transactions of the Royal Society A: Mathematical, Physical and Engineering Sciences **368**(1921), 2937–2960 (2010). URL http://www.scopus.com/inward/record.url?eid=2-s2.0-77954510806&partnerID=40&md5=627533f48335eca268cfaa7112b2a7e4
66. De Lorenzis, L., Temizer, I., Wriggers, P., Zavarise, G.: A large deformation frictional contact formulation using NURBS-based isogeometric analysis. International Journal for Numerical Methods in Engineering **87**(13), 1278–1300 (2011). doi:10.1002/nme.3159. URL http://dx.doi.org/10.1002/nme.3159
67. Deakin, A.: Model for initial vascular patterns in melanoma transplants. Growth **40**(2), 191–201 (1976). URL http://europepmc.org/abstract/MED/1278714
68. Dhote, R.P., Gomez, H., Melnik, R.N.V., Zu, J.: Isogeometric analysis of a dynamic thermo-mechanical phase-field model applied to shape memory alloys. Computational Mechanics **53**(6), 1235–1250 (2014). doi:10.1007/s00466-013-0966-0. URL http://dx.doi.org/10.1007/s00466-013-0966-0
69. Dhote, R.P., Gomez, H., Melnik, R.N.V., Zu, J.: 3D coupled thermo-mechanical phase-field modeling of shape memory alloy dynamics via isogeometric analysis. Computers & Structures **154**, 48 – 58 (2015). doi:10.1016/j.compstruc.2015.02.017. URL http://www.sciencedirect.com/science/article/pii/S0045794915000553
70. Dias Soares Quinas Guerra, M.M., Travasso, R.D.M.: Novel approach to vascular network modeling in 3D. In: Bioengineering (ENBENG), 2012 IEEE 2nd Portuguese Meeting in, pp. 1–6 (2012). doi:10.1109/ENBENG.2012.6331381
71. Dimitri, R., De Lorenzis, L., Wriggers, P., Zavarise, G.: NURBS- and T-spline-based isogeometric cohesive zone modeling of interface debonding. Computational Mechanics **54**(2), 369–388 (2014). doi:10.1007/s00466-014-0991-7. URL http://dx.doi.org/10.1007/s00466-014-0991-7
72. Dimitri, R., Lorenzis, L.D., Scott, M.A., Wriggers, P., Taylor, R.L., Zavarise, G.: Isogeometric large deformation frictionless contact using T-splines. Computer Methods in Applied Mechanics and Engineering **269**, 394 – 414 (2014). doi:10.1016/j.cma.2013.11.002. URL http://www.sciencedirect.com/science/article/pii/S0045782513002971
73. Evans, J.A., Hughes, T.J.R.: Isogeometric divergence-conforming B-splines for the unsteady Navier–Stokes equations. Journal of Computational Physics **241**, 141–167 (2013). doi:10.1016/j.jcp.2013.01.006. URL http://www.sciencedirect.com/science/article/pii/S0021999113000363
74. de Falco, C., Reali, A., Vázquez, R.: GeoPDEs: A research tool for isogeometric analysis of PDEs. Advances in Engineering Software **42**(12), 1020–1034 (2011). doi:10.1016/j.advengsoft.2011.06.010. URL http://www.sciencedirect.com/science/article/pii/S0965997811001839

75. Fentiman, I.S.: Introduction to the Cellular and Molecular Biology of Cancer, chap. Local treatment of cancer, pp. 390–398. Oxford University Press Inc. (2005)
76. Ferlay, J., Soerjomataram, I., Ervik, M., Dikshit, R., Eser, S., Mathers, C., Rebelo, M., Parkin, D., Forman, D., Bray, F.: GLOBOCAN 2012 v1.0, Cancer incidence and mortality worldwide: IARC CancerBase No. 11 (2012). URL http://globocan.iarc.fr
77. Fidler, I.J.: The pathogenesis of cancer metastasis: the "seed and soil" hypothesis revisited. Nature Reviews Cancer **3**(6), 453–458 (2003). doi:10.1038/nrc1098. URL http://www.nature.com/nrc/journal/v3/n6/full/nrc1098.html
78. Fiedler, M.: Algebraic connectivity of graphs. Czechoslovak mathematical journal **23**(2), 298–305 (1973). URL http://hdl.handle.net/10338.dmlcz/101168
79. Figg, W.D., Folkman, J.: Angiogenesis: An integrative approach from science to medicine. Springer (2011)
80. Folkman, J.: Tumor angiogenesis: Therapeutic implications. New England Journal of Medicine **285**(21), 1182–1186 (1971). doi:10.1056/NEJM197111182852108. URL http://www.nejm.org/doi/full/10.1056/NEJM197111182852108
81. Folkman, J., Kalluri, R.: Holland-Frei Cancer Medicine, 6 edn., chap. Tumor angiogenesis, pp. 161–194. BC Decker Inc. (1984)
82. Frieboes, H.B., Jin, F., Chuang, Y.L., Wise, S.M., Lowengrub, J.S., Cristini, V.: Three-dimensional multispecies nonlinear tumor growth-II: Tumor invasion and angiogenesis. Journal of Theoretical Biology **264**(4), 1254–1278 (2010). doi:10.1016/j.jtbi.2010.02.036
83. Frieboes, H.B., Lowengrub, J.S., Wise, S.M., Zheng, X., Macklin, P., Bearer, E.L., Cristini, V.: Computer simulation of glioma growth and morphology. NeuroImage **37**(Suppl. 1), S59–S70 (2007). doi:10.1016/j.neuroimage.2007.03.008
84. Gatenby, R.A., Maini, P.K.: Mathematical oncology: Cancer summed up. Nature **421**(6921), 321–321 (2003). doi:10.1038/421321a. URL http://dx.doi.org/10.1038/421321a
85. Gerhardt, H., Golding, M., Fruttiger, M., Ruhrberg, C., Lundkvist, A., Abramsson, A., Jeltsch, M., Mitchell, C., Alitalo, K., Shima, D., Betsholtz, C.: VEGF guides angiogenic sprouting utilizing endothelial tip cell filopodia. Journal of Cell Biology **161**(6), 1163–1177 (2003). doi:10.1083/jcb.200302047. URL http://jcb.rupress.org/content/161/6/1163.long
86. Gimbrone Jr, M.A., Cotran, R.S., Leapman, S.B., Folkman, J.: Tumor growth and neovascularization: an experimental model using the rabbit cornea. Journal of the National Cancer Institute **52**(2), 699–705 (1974). doi:10.1093/jnci/52.2.413
87. Goel, S., Duda, D.G., Xu, L., Munn, L.L., Boucher, Y., Fukumura, D., Jain, R.K.: Normalization of the vasculature for treatment of cancer and other diseases. Physiological Reviews **91**(3), 1071–1121 (2011). doi:10.1152/physrev.00038.2010. URL http://dx.doi.org/10.1152/physrev.00038.2010
88. Gomez, H., Calo, V.M., Bazilevs, Y., Hughes, T.J.R.: Isogeometric analysis of the Cahn-Hilliard phase-field model. Computer Methods in Applied Mechanics and Engineering **197**(49-50), 4333–4352 (2008). doi:10.1016/j.cma.2008.05.003
89. Graner, F., Glazier, J.A.: Simulation of biological cell sorting using a two-dimensional extended Potts model. Physical Review Letters **69**(13), 2013–2016 (1992). doi:10.1103/PhysRevLett.69.2013
90. Hanahan, D., Weinberg, R.A.: The hallmarks of cancer. Cell **100**(1), 57–70 (2000). doi:10.1016/S0092-8674(00)81683-9. URL http://www.cell.com/abstract/S0092-8674%2800%2981683-9
91. Hanahan, D., Weinberg, R.A.: Hallmarks of cancer: The next generation. Cell **144**(5), 646–674 (2011). doi:10.1016/j.cell.2011.02.013. URL http://www.cell.com/abstract/S0092-8674%2811%2900127-9
92. Harrington, H.A., Maier, M., Naidoo, L., Whitaker, N., Kevrekidis, P.G.: A hybrid model for tumor-induced angiogenesis in the cornea in the presence of inhibitors. Mathematical and Computer Modelling **46**(3-4), 513 – 524 (2007). doi:10.1016/j.mcm.2006.11.034. URL http://www.sciencedirect.com/science/article/pii/S0895717706004249
93. Hawkins-Daarud, A., van der Zee, K.G., Oden, J.T.: Numerical simulation of a thermodynamically consistent four-species tumor growth model. International Journal for Numerical Methods in Biomedical Engineering **28**(1), 3–24 (2012). doi:10.1002/cnm.1467
94. Hellström, M., Phng, L.K., Hofmann, J.J., Wallgard, E., Coultas, L., Lindblom, P., Alva, J., Nilsson, A.K., Karlsson, L., Gaiano, N., Yoon, K., Rossant, J., Iruela-Arispe, M.L., Kalén, M., Gerhardt, H., Betsholtz, C.: Dll4 signalling through Notch1 regulates formation of tip cells during angiogenesis. Nature **445**(7129), 776–

780 (2007). doi:10.1038/nature05571. URL http://www.nature.com/nature/journal/v445/n7129/full/nature05571.html

95. Hill, N.A., Häder, D.P.: A biased random walk model for the trajectories of swimming micro-organisms. Journal of Theoretical Biology **186**(4), 503 – 526 (1997). doi:10.1006/jtbi.1997.0421
96. Hogea, C.S., Murray, B.T., Sethian, J.A.: Simulating complex tumor dynamics from avascular to vascular growth using a general level-set method. Journal of Mathematical Biology **53**(1), 86–134 (2006). doi:10.1007/s00285-006-0378-2
97. Holmes, M.J., Sleeman, B.D.: A mathematical model of tumour angiogenesis incorporating cellular traction and viscoelastic effects. Journal of Theoretical Biology **202**(2), 95–112 (2000). doi:10.1006/jtbi.1999.1038
98. Hughes, T.J.R.: The Finite Element Method: Linear Static and Dynamic Finite Element Analysis. Dover Civil and Mechanical Engineering. Dover Publications (1987)
99. Hughes, T.J.R., Cottrell, J.A., Bazilevs, Y.: Isogeometric analysis: CAD, finite elements, NURBS, exact geometry and mesh refinement. Computer Methods in Applied Mechanics and Engineering **194**(39-41), 4135–4195 (2005). doi:10.1016/j.cma.2004.10.008
100. Hughes, T.J.R., Reali, A., Sangalli, G.: Duality and unified analysis of discrete approximations in structural dynamics and wave propagation: Comparison of ρ-method finite elements with k-method NURBS. Computer Methods in Applied Mechanics and Engineering **197**(49-50), 4104–4124 (2008). doi:10.1016/j.cma.2008.04.006. URL http://www.sciencedirect.com/science/article/pii/S0045782508001618
101. Hughes, T.J.R., Reali, A., Sangalli, G.: Efficient quadrature for NURBS-based isogeometric analysis. Computer Methods in Applied Mechanics and Engineering **199**(5-8), 301–313 (2010). doi:10.1016/j.cma.2008.12.004. URL http://www.sciencedirect.com/science/article/pii/S0045782508004295
102. Jackson, A.M., Porte, J.: Introduction to the Cellular and Molecular Biology of Cancer, chap. Immunotherapy of cancer, pp. 443–457. Oxford University Press Inc. (2005)
103. Jackson, T., Zheng, X.: A cell-based model of endothelial cell migration, proliferation and maturation during corneal angiogenesis. Bulletin of Mathematical Biology **72**(4), 830–868 (2010). doi:10.1007/s11538-009-9471-1. URL http://www.scopus.com/inward/record.url?eid=2-s2.0-77952671503&partnerID=40&md5=e3b49e548303239ed1acde6e3850f58c
104. Jain, R.K.: Normalizing tumor vasculature with anti-angiogenic therapy: A new paradigm for combination therapy. Nature Medicine **7**(9), 987–989 (2001). doi:10.1038/nm0901-987. URL http://dx.doi.org/10.1038/nm0901-987
105. Jain, R.K.: Normalization of tumor vasculature: An emerging concept in antiangiogenic therapy. Science **307**(5706), 58–62 (2005). doi:10.1126/science.1104819. URL http://www.sciencemag.org/content/307/5706/58.abstract
106. Jain, R.K., Munn, L.L., Fukumura, D.: Dissecting tumour pathophysiology using intravital microscopy. Nature Reviews Cancer **2**(4), 266–276 (2002). doi:10.1038/nrc778
107. Jakobsson, L., Franco, C.A., Bentley, K., Collins, R.T., Ponsioen, B., Aspalter, I.M., Rosewell, I., Busse, M., Thurston, G., Medvinsky, A., Schulte-Merker, S., Gerhardt, H.: Endothelial cells dynamically compete for the tip cell position during angiogenic sprouting. Nature Cell Biology **12**(10), 943–953 (2010). doi:10.1038/ncb2103
108. Kadapa, C., Dettmer, W.G., Perić, D.: NURBS based least-squares finite element methods for fluid and solid mechanics. International Journal for Numerical Methods in Engineering **101**(7), 521–539 (2015). doi:10.1002/nme.4765. URL http://dx.doi.org/10.1002/nme.4765
109. Kenyon, B.M., Voest, E.E., Chen, C.C., Flynn, E., Folkman, J., D'Amato, R.J.: A model of angiogenesis in the mouse cornea. Investigative Ophthalmology & Visual Science **37**(8), 1625–1632 (1996). URL http://iovs.arvojournals.org/article.aspx?articleid=2161625
110. Kevrekidis, P.G., Whitaker, N.: Towards a reduced model for angiogenesis: A hybrid approach. Mathematical and Computer Modelling **41**(8-9), 987–996 (2005). doi:10.1016/j.mcm.2004.05.009
111. Kevrekidis, P.G., Whitaker, N., Good, D.J., Herring, G.J.: Minimal model for tumor angiogenesis. Physical Review E **73**(6), 061,926 (2006). doi:10.1103/PhysRevE.73.061926. URL http://www.scopus.com/inward/record.url?eid=2-s2.0-33745614897&partnerID=40&md5=db8a29ab74b57f08bb389ff6d5eddc03
112. Kiendl, J., Bazilevs, Y., Hsu, M.C., Wüchner, R., Bletzinger, K.U.: The bending strip method for isogeometric analysis of Kirchhoff–Love shell structures comprised of multiple patches. Computer Methods in Applied Mechanics and Engineering **199**(37-40), 2403–2416

(2010). doi:10.1016/j.cma.2010.03.029. URL http://www.sciencedirect.com/science/article/pii/S0045782510001064

113. Kilarski, W.W., Samolov, B., Petersson, L., Kvanta, A., Gerwins, P.: Biomechanical regulation of blood vessel growth during tissue vascularization. Nature Medicine **15**(6), 657–664 (2009). doi:10.1038/nm.1985. URL http://dx.doi.org/10.1038/nm.1985
114. Kiltie, A.: Introduction to the Cellular and Molecular Biology of Cancer, chap. Radiotherapy and molecular radiotherapy, pp. 414–427. Oxford University Press Inc. (2005)
115. Kurz, H., Burri, P.H., Djonov, V.G.: Angiogenesis and vascular remodeling by intussusception: From form to function. News in Physiological Sciences **18**(2), 65–70 (2003). doi:10.1152/nips.01417.2002. URL http://physiologyonline.physiology.org/content/18/2/65.long
116. Lee, D.S., Rieger, H., Bartha, K.: Flow correlated percolation during vascular remodeling in growing tumors. Physical Review Letters **96**(5), 058,104 (2006). doi:10.1103/PhysRevLett.96.058104. URL http://link.aps.org/doi/10.1103/PhysRevLett.96.058104
117. Leenders, W.P.J., Küsters, B., de Waal, R.M.W.: Vessel co-option: How tumors obtain blood supply in the absence of sprouting angiogenesis. Endothelium **9**(2), 83–87 (2002). doi:10.1080/10623320212006. URL http://dx.doi.org/10.1080/10623320212006
118. Levine, H.A., Pamuk, S., Sleeman, B.D., Nilsen-Hamilton, M.: Mathematical modeling of capillary formation and development in tumor angiogenesis: Penetration into the stroma. Bulletin of Mathematical Biology **63**(5), 801–863 (2001). doi:10.1006/bulm.2001.0240
119. Levine, H.A., Sleeman, B.D., Nilsen-Hamilton, M.: A mathematical model for the roles of pericytes and macrophages in angiogenesis. I. The role of protease inhibitors in preventing angiogenesis. Mathematical Biosciences **168**(1), 77–115 (2000). doi:10.1016/S0025-5564(00)00034-1
120. Levine, H.A., Sleeman, B.D., Nilsen-Hamilton, M.: Mathematical modeling of the onset of capillary formation initiating angiogenesis. Journal of Mathematical Biology **42**(3), 195–238 (2001). doi:10.1007/s002850000037
121. Levine, H.A., Tucker, A.L., Nilsen-Hamilton, M.: A mathematical model for the role of cell signal transduction in the initiation and inhibition of angiogenesis. Growth Factors **20**(4), 155–175 (2002). doi:10.1080/0897719031000084355
122. Lima, E.A., Oden, J.T., Almeida, R.C.: A hybrid ten-species phase-field model of tumor growth. Mathematical Models and Methods in Applied Sciences **24**(13), 2569–2599 (2014). doi:10.1142/S0218202514500304
123. Liu, G., Qutub, A.A., Vempati, P., Mac Gabhann, F., Popel, A.S.: Module-based multiscale simulation of angiogenesis in skeletal muscle. Theoretical Biology and Medical Modelling **8**(6), 1–26 (2011). doi:10.1186/1742-4682-8-6. URL http://dx.doi.org/10.1186/1742-4682-8-6
124. Liu, J., Gomez, H., Evans, J.A., Hughes, T.J.R., Landis, C.M.: Functional entropy variables: A new methodology for deriving thermodynamically consistent algorithms for complex fluids, with particular reference to the isothermal Navier-Stokes-Korteweg equations. Journal of Computational Physics **248**, 47–86 (2013). doi:10.1016/j.jcp.2013.04.005
125. Liu, J., Landis, C.M., Gomez, H., Hughes, T.J.R.: Liquid–vapor phase transition: Thermomechanical theory, entropy stable numerical formulation, and boiling simulations. Computer Methods in Applied Mechanics and Engineering **In press** (2015). doi:10.1016/j.cma.2015.09.007. URL http://www.sciencedirect.com/science/article/pii/S0045782515003011
126. Loeb, L.A., Loeb, K.R., Anderson, J.P.: Multiple mutations and cancer. Proceedings of the National Academy of Sciences **100**(3), 776–781 (2003). doi:10.1073/pnas.0334858100
127. Logsdon, E.A., Finley, S.D., Popel, A.S., Mac Gabhann, F.: A systems biology view of blood vessel growth and remodelling. Journal of Cellular and Molecular Medicine **18**(8), 1491–1508 (2014). doi:10.1111/jcmm.12164
128. Lowengrub, J.S., Frieboes, H.B., Jin, F., Chuang, Y.L., Li, X., Macklin, P., Wise, S.M., Cristini, V.: Nonlinear modelling of cancer: Bridging the gap between cells and tumours. Nonlinearity **23**(1), R1–R9 (2010). doi:10.1088/0951-7715/23/1/R01. URL http://iopscience.iop.org/article/10.1088/0951-7715/23/1/R01/meta
129. Mahoney, A.W., Smith, B.G., Flann, N.S., Podgorski, G.J.: Discovering novel cancer therapies: A computational modeling and search approach. In: Computational Intelligence in Bioinformatics and Computational Biology, 2008. CIBCB '08. IEEE Symposium on, pp. 233–240 (2008). doi:10.1109/CIBCB.2008.4675785
130. Mancuso, M.R., Davis, R., Norberg, S.M., O'Brien, S., Sennino, B., Nakahara, T., Yao, V.J., Inai, T., Brooks, P., Freimark, B., Shalinsky, D.R., Hu-Lowe,

D.D., McDonald, D.M.: Rapid vascular regrowth in tumors after reversal of VEGF inhibition. Journal of Clinical Investigation **116**(10), 2610–2621 (2006). doi:10.1172/JCI24612. URL http://www.ncbi.nlm.nih.gov/pmc/articles/PMC1578604/

131. Mantzaris, N.V., Webb, S., Othmer, H.G.: Mathematical modeling of tumor-induced angiogenesis. Journal of Mathematical Biology **49**(2), 111–187 (2004). doi:10.1007/s00285-003-0262-2
132. Matsumoto, S., Yasui, H., Batra, S., Kinoshita, Y., Bernardo, M., Munasinghe, J.P., Utsumi, H., Choudhuri, R., Devasahayam, N., Subramanian, S., Mitchell, J.B., Krishna, M.C.: Simultaneous imaging of tumor oxygenation and microvascular permeability using overhauser enhanced mri. Proceedings of the National Academy of Sciences **106**(42), 17,898–17,903 (2009). doi:10.1073/pnas.0908447106. URL http://www.pnas.org/content/106/42/17898.abstract
133. McDonald, D.M., Choyke, P.L.: Imaging of angiogenesis: from microscope to clinic. Nature Medicine **9**(6), 713–725 (2003). doi:10.1038/nm0603-713. URL http://dx.doi.org/10.1038/nm0603-713
134. McDougall, S.R., Anderson, A.R.A., Chaplain, M.A.J.: Mathematical modelling of dynamic adaptive tumour-induced angiogenesis: Clinical implications and therapeutic targeting strategies. Journal of Theoretical Biology **241**(3), 564–589 (2006). doi:10.1016/j.jtbi.2005.12.022. URL http://dx.doi.org/10.1016/j.jtbi.2005.12.022
135. McDougall, S.R., Anderson, A.R.A., Chaplain, M.A.J., Sherrat, J.A.: Mathematical modelling of flow through vascular networks: Implications for tumour-induced angiogenesis and chemotherapy strategies. Bulletin of Mathematical Biology **64**(4), 673–702 (2002). doi:10.1006/bulm.2002.0293
136. McDougall, S.R., Watson, M.G., Devlin, A.H., Mitchell, C.A., Chaplain, M.A.J.: A hybrid discrete-continuum mathematical model of pattern prediction in the developing retinal vasculature. Bulletin of Mathematical Biology **74**(10), 2272–2314 (2012). doi:10.1007/s11538-012-9754-9
137. Milde, F., Bergdorf, M., Koumoutsakos, P.: A hybrid model for three-dimensional simulations of sprouting angiogenesis. Biophysical Journal **95**(7), 3146–3160 (2008). doi:h10.1529/biophysj.107.124511. URL http://www.sciencedirect.com/science/article/pii/S0006349508784595
138. Moreira, J., Deutsch, A.: Cellular automaton models of tumor development: A critical review. Advances in Complex Systems **5**(2-3), 247–267 (2002). doi:10.1142/S0219525902000572
139. Morganti, S., Auricchio, F., Benson, D.J., Gambarin, F.I., Hartmann, S., Hughes, T.J.R., Reali, A.: Patient-specific isogeometric structural analysis of aortic valve closure. Computer Methods in Applied Mechanics and Engineering **284**, 508–520 (2015). doi:10.1016/j.cma.2014.10.010. URL http://www.sciencedirect.com/science/article/pii/S0045782514003806
140. Muthukkaruppan, V.R., Kubai, L., Auerbach, R.: Tumor-induced neovascularization in the mouse eye. Journal of the National Cancer Institute **69**(3), 699–708 (1982). doi:10.1093/jnci/69.3.699
141. Nagy, J., Dvorak, H.: Heterogeneity of the tumor vasculature: the need for new tumor blood vessel type-specific targets. Clinical & Experimental Metastasis **29**(7), 657–662 (2012). doi:10.1007/s10585-012-9500-6. URL http://dx.doi.org/10.1007/s10585-012-9500-6
142. Nguyen-Thanh, N., Nguyen-Xuan, H., Bordas, S.P.A., Rabczuk, T.: Isogeometric analysis using polynomial splines over hierarchical T-meshes for two-dimensional elastic solids. Computer Methods in Applied Mechanics and Engineering **200**(21-22), 1892–1908 (2011). doi:10.1016/j.cma.2011.01.018. URL http://www.sciencedirect.com/science/article/pii/S0045782511000338
143. Oden, J.T., Lima, E.A.B.F., Almeida, R.C., Feng, Y., Rylander, M.N., Fuentes, D., Faghihi, D., Rahman, M.M., DeWitt, M., Gadde, M., Zhou, J.C.: Toward predictive multiscale modeling of vascular tumor growth. Archives of Computational Methods in Engineering pp. 1–45 (2015). doi:10.1007/s11831-015-9156-x. URL http://dx.doi.org/10.1007/s11831-015-9156-x
144. Oden, J.T., Prudencio, E.E., Hawkins-Daarud, A.: Selection and assessment of phenomenological models of tumor growth. Mathematical Models and Methods in Applied Sciences **23**(7), 1309–1338 (2013). doi:10.1142/S0218202513500103
145. Olsen, L., Sherratt, J.A., Maini, P.K., Arnold, F.: A mathematical model for the capillary endothelial cell-extracellular matrix interactions in wound-healing angiogenesis. Mathematical Medicine and Biology **14**(4), 261–281 (1997). doi:10.1093/imammb/14.4.261. URL http://imammb.oxfordjournals.org/content/14/4/261.abstract
146. Orme, M.E., Chaplain, M.A.J.: A mathematical model of the first steps of tumour-related angiogenesis: Capillary sprout formation and secondary branching. IMA Journal of Mathematics Ap-

plied in Medicine and Biology **13**(2), 73–98 (1996). doi:10.1093/imammb/13.2.73
147. Orme, M.E., Chaplain, M.A.J.: A mathematical model of vascular tumour growth and invasion. Mathematical and Computer Modelling **23**(10), 43 – 60 (1996). doi:10.1016/0895-7177(96)00053-2
148. Orme, M.E., Chaplain, M.A.J.: Two-dimensional models of tumour angiogenesis and anti-angiogenesis strategies. Mathematical Medicine and Biology **14**(3), 189–205 (1997). doi:10.1093/imammb/14.3.189
149. Pauletti, M.S., Martinelli, M., Cavallini, N., Antolin, P.: Igatools: An isogeometric analysis library. SIAM Journal on Scientific Computing **37**(4), C465–C496 (2015). doi:10.1137/140955252
150. Perfahl, H., Byrne, H.M., Chen, T., Estrella, V., Alarcón, T., Lapin, A., Gatenby, R.A., Gillies, R.J., Lloyd, M.C., Maini, P.K., Reuss, M., Owen, M.R.: Multiscale modelling of vascular tumour growth in 3D: The roles of domain size and boundary conditions. PLoS ONE **6**(4), e14,790 (2011). doi:10.1371/journal.pone.0014790. URL http://dx.doi.org/10.1371/journal.pone.0014790
151. Peterson, J.W., Carey, G.F., Knezevic, D.J., Murray, B.T.: Adaptive finite element methodology for tumour angiogenesis modelling. International Journal for Numerical Methods in Engineering **69**(6), 1212–1238 (2007). doi:10.1002/nme.1802. URL http://dx.doi.org/10.1002/nme.1802
152. Phipps, C., Kohandel, M.: Mathematical model of the effect of interstitial fluid pressure on angiogenic behavior in solid tumors. Computational and Mathematical Methods in Medicine **2011**(Article ID 843765), 1–9 (2011). doi:10.1155/2011/843765. URL http://dx.doi.org/10.1155/2011/843765
153. Piegl, L., Tiller, W.: The NURBS Book. Springer-Verlag Berlin Heidelberg (1997)
154. Plank, M.J., Sleeman, B.D.: A reinforced random walk model of tumour angiogenesis and anti-angiogenic strategies. Mathematical Medicine and Biology **20**(2), 135–181 (2003). doi:10.1093/imammb/20.2.135
155. Plank, M.J., Sleeman, B.D.: Lattice and non-lattice models of tumour angiogenesis. Bulletin of Mathematical Biology **66**(6), 1785–1819 (2004). doi:10.1016/j.bulm.2004.04.001
156. Plank, M.J., Sleeman, B.D., Jones, P.F.: A mathematical model of tumour angiogenesis, regulated by vascular endothelial growth factor and the angiopoietins. Journal of Theoretical Biology **229**(4), 435 – 454 (2004). doi:10.1016/j.jtbi.2004.04.012. URL http://www.sciencedirect.com/science/article/pii/S0022519304001535
157. Potente, M., Gerhardt, H., Carmeliet, P.: Basic and therapeutic aspects of angiogenesis. Cell **146**(6), 873–887 (2011). doi:10.1016/j.cell.2011.08.039. URL http://dx.doi.org/10.1016/j.cell.2011.08.039
158. Pries, A.R., Reglin, B., Secomb, T.W.: Structural adaptation of microvascular networks: functional roles of adaptive responses. American Journal of Physiology - Heart and Circulatory Physiology **281**(3), H1015–H1025 (2001). URL http://ajpheart.physiology.org/content/281/3/H1015
159. Pries, A.R., Secomb, T.W., Gaehtgens, P.: Biophysical aspects of blood flow in the microvasculature. Cardiovascular Research **32**(4), 654–667 (1996). doi:10.1016/S0008-6363(96)00065-X 654-667. URL http://cardiovascres.oxfordjournals.org/content/32/4/654.long
160. Pries, A.R., Secomb, T.W., Gaehtgens, P.: Structural adaptation and stability of microvascular networks: theory and simulations. American Journal of Physiology - Heart and Circulatory Physiology **275**(2), H349–H360 (1998). URL http://ajpheart.physiology.org/content/275/2/H349
161. Pries, A.R., Secomb, T.W., Gaehtgens, P., Gross, J.F.: Blood flow in microvascular networks: Experiments and simulation. Circulation Research **67**(4), 826–834 (1990). doi:10.1161/01.RES.67.4.826. URL http://circres.ahajournals.org/content/67/4/826.short
162. Pries, A.R., Secomb, T.W., Geβner, T., Sperandio, M.B., Gross, J.F., Gaehtgens, P.: Resistance to blood and flow in microvessels and in vivo. Circulation Research **75**(5), 904–915 (1994). doi:10.1161/01.RES.75.5.904. URL http://circres.ahajournals.org/content/75/5/904.abstract
163. Qutub, A.A., Mac Gabhann, F., Karagiannis, E.D., Vempati, P., Popel, A.S.: Multiscale models of angiogenesis. Engineering in Medicine and Biology Magazine, IEEE **28**(2), 14 –31 (2009). doi:10.1109/MEMB.2009.931791
164. Reali, A., Gomez, H.: An isogeometric collocation approach for Bernoulli–Euler beams and Kirchhoff plates. Computer Methods in Applied Mechanics and Engineering **284**, 623 – 636 (2015). doi:10.1016/j.cma.2014.10.027. URL http://www.sciencedirect.com/science/article/pii/S0045782514003971
165. Reina-Romo, E., Valero, C., Borau, C., Rey, R., Javierre, E., Gómez-Benito, M.J., Domínguez, J.,

García-Aznar, J.M.: Mechanobiological modelling of angiogenesis: Impact on tissue engineering and bone regeneration. In: L. Geris (ed.) Computational Modeling in Tissue Engineering, *Studies in Mechanobiology, Tissue Engineering and Biomaterials*, vol. 10, pp. 379–404. Springer Berlin Heidelberg (2013). doi:10.1007/8415_2011_111. URL http://dx.doi.org/10.1007/8415_2011_111

166. Rogers, D.F.: An Introduction to NURBS: With Historical Perspective. Morgan Kaufmann Publishers Inc., San Francisco, CA, USA (2001)
167. Roose, T., Chapman, S.J., Maini, P.K.: Mathematical models of avascular tumor growth. SIAM Reviews **49**(2), 179–208 (2007). doi:10.1137/S0036144504446291
168. Roussos, E.T., Condeelis, J.S., Patsialou, A.: Chemotaxis in cancer. Nature Reviews Cancer **11**(8), 573–587 (2011). doi:10.1038/nrc3078
169. Saeed, K., Tabedzki, M., Rybnik, M., Adamski, M.: K3M: A universal algorithm for image skeletonization and a review of thinning techniques. International Journal of Applied Mathematics and Computer Science **20**(2), 317–355 (2010). doi:10.2478/v10006-010-0024-4
170. Sanga, S., Frieboes, H.B., Zheng, X., Gatenby, R., Bearer, E.L., Cristini, V.: Predictive oncology: A review of multidisciplinary, multiscale in silico modeling linking phenotype, morphology and growth. NeuroImage **37**(Supplement 1), S120 – S134 (2007). doi:10.1016/j.neuroimage.2007.05.043. URL http://www.sciencedirect.com/science/article/pii/S1053811907004946
171. Sanga, S., Sinek, J.P., Frieboes, H.B., Ferrari, M., Fruehauf, J.P., Cristini, V.: Mathematical modeling of cancer progression and response to chemotherapy. Expert Review of Anticancer Therapy **6**(10), 1361–1376 (2006). doi:10.1586/14737140.6.10.1361. URL http://dx.doi.org/10.1586/14737140.6.10.1361
172. Santos-Oliveira, P., Correia, A., Rodrigues, T., Ribeiro-Rodrigues, T.M., Matafome, P., Rodríguez-Manzaneque, J.C., Seiça, R., Girão, H., Travasso, R.D.M.: The force at the tip - Modelling tension and proliferation in sprouting angiogenesis. PLoS Computational Biology **11**(8), e1004,436 (2015). doi:10.1371/journal.pcbi.1004436. URL http://dx.doi.org/10.1371%2Fjournal.pcbi.1004436
173. Schillinger, D., Dedé, L., Scott, M.A., Evans, J.A., Borden, M.J., Rank, E., Hughes, T.J.R.: An isogeometric design-through-analysis methodology based on adaptive hierarchical refinement of NURBS, immersed boundary methods, and T-spline CAD surfaces. Computer Methods in Applied Mechanics and Engineering **249-252**, 116–150 (2012). doi:10.1016/j.cma.2012.03.017. URL http://www.sciencedirect.com/science/article/pii/S004578251200093X
174. Schmidt, R., Wüchner, R., Bletzinger, K.U.: Isogeometric analysis of trimmed NURBS geometries. Computer Methods in Applied Mechanics and Engineering **241-244**, 93–111 (2012). doi:10.1016/j.cma.2012.05.021. URL http://www.sciencedirect.com/science/article/pii/S0045782512001843
175. Scianna, M., Bell, C.G., Preziosi, L.: A review of mathematical models for the formation of vascular networks. Journal of Theoretical Biology **333**, 174–209 (2013). doi:10.1016/j.jtbi.2013.04.037
176. Scott, M.A., Thomas, D.C., Evans, E.J.: Isogeometric spline forests. Computer Methods in Applied Mechanics and Engineering **269**, 222–264 (2014). doi:10.1016/j.cma.2013.10.024. URL http://www.sciencedirect.com/science/article/pii/S0045782513002764
177. Secomb, T.W., Alberding, J.P., Hsu, R., Dewhirst, M.W., Pries, A.R.: Angiogenesis: An adaptive dynamic biological patterning problem. PLoS Computational Biology **9**(3), e1002,983 (2013). doi:10.1371/journal.pcbi.1002983. URL http://dx.doi.org/10.1371/journal.pcbi.1002983
178. Secomb, T.W., Pries, A.R.: The microcirculation: physiology at the mesoscale. The Journal of Physiology **589**(5), 1047–1052 (2011). doi:10.1113/jphysiol.2010.201541. URL http://dx.doi.org/10.1113/jphysiol.2010.201541
179. Shan, S., Lockhart, A.C., Saito, W.Y., Knapp, A.M., Laderoute, K.R., Dewhirst, M.W.: The novel tubulin-binding drug bto-956 inhibits r3230ac mammary carcinoma growth and angiogenesis in fischer 344 rats. Clinical Cancer Research **7**(8), 2590–2596 (2001). URL http://clincancerres.aacrjournals.org/content/7/8/2590.abstract
180. Shirinifard, A., Gens, J.S., Zaitlen, B.L., Popławski, N.J., Swat, M., Glazier, J.A.: 3D multi-cell simulation of tumor growth and angiogenesis. PLoS ONE **4**(10), e7190 (2009). doi:10.1371/journal.pone.0007190
181. Sleeman, B., Wallis, I.P.: Tumour induced angiogenesis as a reinforced random walk: Modelling capillary network formation without endothelial cell proliferation. Mathematical and Computer Modelling **36**(3), 339–358 (2002). doi:10.1016/S0895-7177(02)00129-2

182. Speleers, H., Manni, C., Pelosi, F., Sampoli, M.L.: Isogeometric analysis with Powell–Sabin splines for advection–diffusion–reaction problems. Computer Methods in Applied Mechanics and Engineering **221-222**, 132–148 (2012). doi:10.1016/j.cma.2012.02.009. URL http://www.sciencedirect.com/science/article/pii/S0045782512000515
183. Stamper, I.J., Byrne, H.M., Owen, M.R., Maini, P.K.: Modelling the role of angiogenesis and vasculogenesis in solid tumour growth. Bulletin of Mathematical Biology **69**(8), 2737–2772 (2007). doi:10.1007/s11538-007-9253-6. URL http://dx.doi.org/10.1007/s11538-007-9253-6
184. Stéphanou, A., McDougall, S.R., Anderson, A.R.A., Chaplain, M.A.J.: Mathematical modelling of flow in 2D and 3D vascular networks: Applications to anti-angiogenic and chemotherapeutic drug strategies. Mathematical and Computer Modelling **41**(10), 1137–1156 (2005). doi:10.1016/j.mcm.2005.05.008
185. Stéphanou, A., McDougall, S.R., Anderson, A.R.A., Chaplain., M.A.J.: Mathematical modelling of the influence of blood rheological properties upon adaptative tumour-induced angiogenesis. Mathematical and Computer Modelling **44**(1-2), 96–123 (2006). doi:10.1016/j.mcm.2004.07.021. URL http://dx.doi.org/10.1016/j.mcm.2004.07.021
186. Stokes, C.L., Lauffenburger, D.A.: Analysis of the roles of microvessel endothelial cell random motility and chemotaxis in angiogenesis. Journal of Theoretical Biology **152**(3), 377–403 (1991). doi:10.1016/S0022-5193(05)80201-2
187. Sun, S., Wheeler, M.F., Obeyesekere, M., Patrick, C.W.: A deterministic model of growth factor-induced angiogenesis. Bulletin of Mathematical Biology **67**(2), 313–337 (2005). doi:10.1016/j.bulm.2004.07.004
188. Szabó, A., Czirók, A.: The role of cell-cell adhesion in the formation of multicellular sprouts. Mathematical Modelling of Natural Phenomena **5**(1), 106–122 (2010). doi:10.1051/mmnp/20105105. URL http://dx.doi.org/10.1051/mmnp/20105105
189. Szabó, A., Mehes, E., Kosa, E., Czirók, A.: Multicellular sprouting in vitro. Biophysical Journal **95**(6), 2702 – 2710 (2008). doi:10.1529/biophysj.108.129668. URL http://www.sciencedirect.com/science/article/pii/S0006349508784157
190. Talmadge, J.E., Fidler, I.J.: AACR centennial series: the biology of cancer metastasis: historical perspective. Cancer Research **79**, 5649–5669 (2010). doi:10.1158/0008-5472.CAN-10-1040. URL http://cancerres.aacrjournals.org/content/70/14/5649
191. Taylor, C.A., Figueroa, C.A.: Patient-specific modeling of cardiovascular mechanics. Annual Review of Biomedical Engineering **11**(1), 109–134 (2009). doi:10.1146/annurev.bioeng.10.061807.160521. URL http://dx.doi.org/10.1146/annurev.bioeng.10.061807.160521
192. Taylor, M., Prendergast, P.J.: Four decades of finite element analysis of orthopaedic devices: Where are we now and what are the opportunities? Journal of Biomechanics **48**(5), 767 – 778 (2015). doi:10.1016/j.jbiomech.2014.12.019. URL http://www.sciencedirect.com/science/article/pii/S0021929014006733
193. Tong, S., Yuan, F.: Numerical simulations of angiogenesis in the cornea. Microvascular Research **61**(1), 14–27 (2001). doi:10.1006/mvre.2000.2282. URL http://www.scopus.com/inward/record.url?eid=2-s2.0-0034757316&partnerID=40&md5=b81b95701c51eb602e819fe0df9a8ec6
194. Tong, S., Yuan, F.: Dose response of angiogenesis to basic fibroblast growth factor in rat corneal pocket assay: II. numerical simulations. Microvascular Research **75**(1), 16 – 24 (2008). doi:10.1016/j.mvr.2007.09.005. URL http://www.sciencedirect.com/science/article/pii/S002628620700115X
195. Travasso, R.D.M., Castro, M., Oliveira, J.C.R.E.: The phase-field model in tumor growth. Philosophical Magazine **91**(1), 183–206 (2011). doi:10.1080/14786435.2010.501771. URL http://www.tandfonline.com/doi/abs/10.1080/14786435.2010.501771
196. Travasso, R.D.M., Corvera Poiré, E., Castro, M., Rodríguez-Manzaneque, J.C., Hernández-Machado, A.: Tumor angiogenesis and vascular patterning: A mathematical model. PLoS ONE **6**(5), e19,989 (2011). doi:10.1371/journal.pone.0019989
197. Valenciano, J., Chaplain, M.A.J.: An explicit subparametric spectral element method of lines applied to a tumour angiogenesis system of partial differential equations. Mathematical Models and Methods in Applied Sciences **14**(2), 165–187 (2004). doi:10.1142/S0218202504003155. URL http://www.worldscientific.com/doi/abs/10.1142/S0218202504003155
198. Valero, C., Javierre, E., García-Aznar, J.M., Gómez-Benito, M.J.: Numerical modelling of the angiogenesis process in wound contraction. Biomechanics and Modeling in Mechanobiology **12**(2), 349–360 (2013).

doi:10.1007/s10237-012-0403-x. URL http://dx.doi.org/10.1007/s10237-012-0403-x

199. Valero, C., Javierre, E., García-Aznar, J.M., Gómez-Benito, M.J., Menzel, A.: Modeling of anisotropic wound healing. Journal of the Mechanics and Physics of Solids **79**, 80 – 91 (2015). doi:10.1016/j.jmps.2015.03.009. URL http://www.sciencedirect.com/science/article/pii/S0022509615000654
200. Valero, C., Javierre, E., García-Aznar, J.M., Menzel, A., Gómez-Benito, M.J.: Challenges in the modeling of wound healing mechanisms in soft biological tissues. Annals of Biomedical Engineering **43**(7), 1654–1665 (2015). doi:10.1007/s10439-014-1200-8. URL http://dx.doi.org/10.1007/s10439-014-1200-8
201. Vermolen, F.J., Javierre, E.: A finite-element model for healing of cutaneous wounds combining contraction, angiogenesis and closure. Journal of Mathematical Biology **65**(5), 967–996 (2012). doi:10.1007/s00285-011-0487-4. URL http://dx.doi.org/10.1007/s00285-011-0487-4
202. Vilanova, G., Colominas, I., Gomez, H.: Capillary networks in tumor angiogenesis: From discrete endothelial cells to phase-field averaged descriptions via isogeometric analysis. International Journal for Numerical Methods in Biomedical Engineering **29**(10), 1015–1037 (2013). doi:10.1002/cnm.2552. URL http://dx.doi.org/10.1002/cnm.2552
203. Vilanova, G., Colominas, I., Gomez, H.: Coupling of discrete random walks and continuous modeling for three-dimensional tumor-induced angiogenesis. Computational Mechanics **53**(3), 449–464 (2014). doi:10.1007/s00466-013-0958-0. URL http://dx.doi.org/10.1007/s00466-013-0958-0
204. Wall, W.A., Frenzel, M.A., Cyron, C.: Isogeometric structural shape optimization. Computer Methods in Applied Mechanics and Engineering **197**(33-40), 2976–2988 (2008). doi:10.1016/j.cma.2008.01.025. URL http://www.sciencedirect.com/science/article/pii/S0045782508000509
205. Weinberg, R.: One renegade cell: How cancer begins. Basic Books (1998)
206. Weis, S.M., Cheresh, D.A.: Tumor angiogenesis: molecular pathways and therapeutic targets. Nature Medicine **17**(11), 1359–1370 (2011). doi:10.1038/nm.2537. URL http://dx.doi.org/10.1038/nm.2537
207. Welter, M., Bartha, K., Rieger, H.: Emergent vascular network inhomogeneities and resulting blood flow patterns in a growing tumor. Journal of Theoretical Biology **250**(2), 257–280 (2008). doi:10.1016/j.jtbi.2007.09.031. URL http://dx.doi.org/10.1016/j.jtbi.2007.09.031
208. Welter, M., Bartha, K., Rieger, H.: Vascular remodelling of an arterio-venous blood vessel network during solid tumour growth. Journal of Theoretical Biology **259**(3), 405–422 (2009). doi:10.1016/j.jtbi.2009.04.005. URL http://dx.doi.org/10.1016/j.jtbi.2009.04.005
209. Welter, M., Rieger, H.: Physical determinants of vascular network remodeling during tumor growth. The European Physical Journal E **33**(2), 149–163 (2010). doi:10.1140/epje/i2010-10611-6. URL http://dx.doi.org/10.1140/epje/i2010-10611-6
210. Welter, M., Rieger, H.: Interstitial fluid flow and drug delivery in vascularized tumors: A computational model. PLoS ONE **8**(8), e70,395 (2013). doi:10.1371/journal.pone.0070395
211. Wise, S.M., Lowengrub, J.S., Frieboes, H.B., Cristini, V.: Three-dimensional multispecies nonlinear tumor growth-I: Model and numerical method. Journal of Theoretical Biology **253**(3), 524–543 (2008). doi:10.1016/j.jtbi.2008.03.027
212. World Bank: World development indicators (2014). doi:10.1596/978-1-4648-0163-1. URL www.worldbank.org
213. Wu, J., Long, Q., Xu, S., Padhani, A.R.: Study of tumor blood perfusion and its variation due to vascular normalization by anti-angiogenic therapy based on 3D angiogenic microvasculature. Journal of Biomechanics **42**(6), 712–721 (2009). doi:10.1016/j.jbiomech.2009.01.009
214. Wu, J., Xu, S., Long, Q., Collins, M.W., König, C.S., Zhao, G., Jiang, Y., Padhani, A.R.: Coupled modeling of blood perfusion in intravascular, interstitial spaces in tumor microvasculature. Journal of Biomechanics **41**(5), 996–1004 (2008). doi:10.1016/j.jbiomech.2007.12.008. URL http://dx.doi.org/10.1016/j.jbiomech.2007.12.008
215. Wu, M., Frieboes, H.B., McDougall, S.R., Chaplain, M.A.J., Cristini, V., Lowengrub, J.: The effect of interstitial pressure on tumor growth: Coupling with the blood and lymphatic vascular systems. Journal of Theoretical Biology **320**, 131–151 (2013). doi:10.1016/j.jtbi.2012.11.031. URL http://dx.doi.org/10.1016/j.jtbi.2012.11.031
216. Xia, S., Wang, X., Qian, X.: Continuity and convergence in rational triangular Bézier spline based isogeometric analysis. Computer Methods in Applied Mechanics and Engineering **In press** (2015). doi:10.1016/j.cma.2015.09.001. URL http://www.sciencedirect.com/science/article/pii/S0045782515002777

217. Xu, J., Vilanova, G., Gomez, H.: A mathematical model coupling tumor growth and angiogenesis. PLoS ONE **11**(2), e0149,422 (2016). doi:10.1371/journal.pone.0149422. URL http://dx.doi.org/10.1371%2Fjournal.pone.0149422
218. Xu, J., Vilanova, G., Gomez, H.: Full-scale, three-dimensional simulation of early-stage tumor growth: The onset of malignancy. Computer Methods in Applied Mechanics and Engineering **314**, 126 – 146 (2017). doi:http://dx.doi.org/10.1016/j.cma.2016.07.010. URL http://www.sciencedirect.com/science/article/pii/S0045782516307368
219. Yankeelov, T.E., An, G., Saut, O., Luebeck, E.G., Popel, A.S., Ribba, B., Vicini, P., Zhou, X., Weis, J.A., Ye, K., Genin, G.M.: Multi-scale modeling in clinical oncology: Opportunities and barriers to success. Annals of Biomedical Engineering **44**(9), 2626–2641 (2016). doi:10.1007/s10439-016-1691-6. URL http://dx.doi.org/10.1007/s10439-016-1691-6
220. Yankeelov, T.E., Atuegwu, N., Hormuth, D., Weis, J.A., Barnes, S.L., Miga, M.I., Rericha, E.C., Quaranta, V.: Clinically relevant modeling of tumor growth and treatment response. Science translational medicine **5**(187), 187ps9–187ps9 (2013)
221. Yu, P., Mustata, M., Peng, L., Turek, J.J., Melloch, M.R., French, P.M.W., Nolte, D.D.: Holographic optical coherence imaging of rat osteogenic sarcoma tumor spheroids. Applied Optics **43**(25), 4862–4873 (2004). doi:10.1364/AO.43.004862. URL http://ao.osa.org/abstract.cfm?URI=ao-43-25-4862
222. Zhang, T.Y., Suen, C.Y.: A fast parallel algorithm for thinning digital patterns. Communications of the ACM **27**(3), 236–239 (1984). doi:10.1145/357994.358023
223. Zheng, X., Wise, S.M., Cristini, V.: Nonlinear simulation of tumor necrosis, neo-vascularization and tissue invasion via an adaptive finite-element/level-set method. Bulletin of Mathematical Biology **67**(2), 211–259 (2005). doi:10.1016/j.bulm.2004.08.001